

ALSHAMMARI, A.F., ZATTARIN, A., PEARSON, A., CRUICKSHANK, E., MAJEWSKA, M., POCIECHA, D., STOREY, J.M.D., GORECKA, E., IMRIE, C.T. and WALKER, R. 2024. Heliconical nematic and smectic phases: the synthesis and characterisation of the CB4O.m and CB8O.m series. *Liquid crystals* [online], 51(13-14): proceedings of the 16th European conference on liquid crystals (ECLC 2023), 10-14 July 2023, Rende, Italy, pages 2300-2312. Available from: <https://doi.org/10.1080/02678292.2024.2334342>

Heliconical nematic and smectic phases: the synthesis and characterisation of the CB4O.m and CB8O.m series.

ALSHAMMARI, A.F., ZATTARIN, A., PEARSON, A., CRUICKSHANK, E., MAJEWSKA, M., POCIECHA, D., STOREY, J.M.D., GORECKA, E., IMRIE, C.T. and WALKER, R.

2024

© 2024 The Author(s). Published by Informa UK Limited, trading as Taylor & Francis Group.
Supplementary materials are appended after the main text of this document.



Heliconical nematic and smectic phases: the synthesis and characterisation of the CB4O.*m* and CB8O.*m* series

Ahlam F Alshammari, Amerigo Zattarin, Abigail Pearson, Ewan Cruickshank, Magdalena Majewska, Damian Pocięcha, John MD Storey, Ewa Gorecka, Corrie T. Imrie & Rebecca Walker

To cite this article: Ahlam F Alshammari, Amerigo Zattarin, Abigail Pearson, Ewan Cruickshank, Magdalena Majewska, Damian Pocięcha, John MD Storey, Ewa Gorecka, Corrie T. Imrie & Rebecca Walker (2024) Heliconical nematic and smectic phases: the synthesis and characterisation of the CB4O.*m* and CB8O.*m* series, Liquid Crystals, 51:13-14, 2300-2312, DOI: [10.1080/02678292.2024.2334342](https://doi.org/10.1080/02678292.2024.2334342)

To link to this article: <https://doi.org/10.1080/02678292.2024.2334342>



© 2024 The Author(s). Published by Informa UK Limited, trading as Taylor & Francis Group.



[View supplementary material](#)



Published online: 18 Apr 2024.



[Submit your article to this journal](#)



Article views: 882



[View related articles](#)



[View Crossmark data](#)



Citing articles: 1 [View citing articles](#)

Heliconical nematic and smectic phases: the synthesis and characterisation of the CB40.*m* and CB80.*m* series

Ahlam F Alshammari^a, Amerigo Zattarin^a, Abigail Pearson^a, Ewan Cruickshank^{a,b}, Magdalena Majewska^c, Damian Pociecha^c, John MD Storey^a, Ewa Gorecka^c, Corrie T. Imrie^a and Rebecca Walker^a

^aDepartment of Chemistry, School of Natural and Computing Sciences, University of Aberdeen, Aberdeen, UK; ^bSchool of Pharmacy and Life Sciences, Robert Gordon University, Aberdeen, UK; ^cFaculty of Chemistry, University of Warsaw, Warsaw, Poland

ABSTRACT

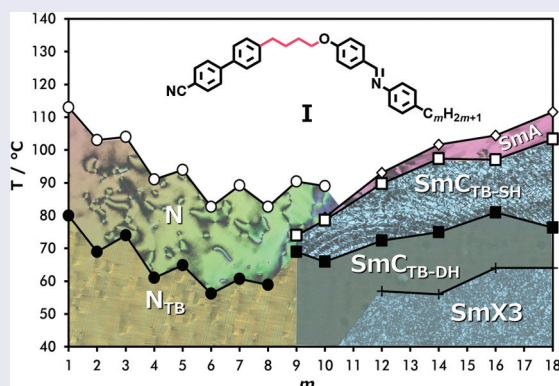
The synthesis and characterisation of two series of nonsymmetric dimers belonging to the family of compounds, the 1-(4-cyanobiphenyl-4'-yl)- ω -(4-alkylanilinebenzylidene-4'-oxy)alkanes (CB*n*O.*m*) is reported; in the acronym, *n* refers to the number of carbon atoms in the spacer, and *m* in the terminal alkyl chain. The two series reported, CB40.*m* and CB80.*m*, both show twist-bend nematic (*N*_{TB}) and smectic phases (SmC_{TB-SH} and SmC_{TB-DH}). Their phase behaviour is compared to that of the CB60.*m* and CB100.*m* series. For each series, locally intercalated molecular packing is observed for short terminal chains and interdigitated packing for long terminal chains. The intercalated anticlinic smectic C_A phase is observed for the CB80.*m* and CB100.*m* series. All four series exhibit the SmC_{TB-SH} and SmC_{TB-DH} phases for the longer terminal chains and all have an interdigitated molecular arrangement. The absence of an intercalated heliconical phase is attributed to the high viscosity associated with the network intercalated structure.

ARTICLE HISTORY

Received 15 December 2023
Accepted 5 March 2024

KEYWORDS

Heliconical smectic phases;
twist-bend smectics; twist-bend nematic phase;
cyanobiphenyls; liquid crystal dimers




Introduction

Dimeric liquid crystals consist of molecules containing two semi-rigid mesogenic moieties linked *via* a flexible spacer, normally an alkyl chain [1]. The parity of the spacer governs the average shape of the dimer such that if an even number of atoms connect the two mesogenic units the molecule is linear, whereas for an odd number of atoms, the molecule is bent. Bent, odd-membered dimers have attracted considerable research attention in recent years due to their ability to form a new class of liquid crystal phases in which the director adopts

a heliconical distribution, the twist-bend phases [2]. The least ordered of these phases is the twist-bend nematic phase (*N*_{TB}), first proposed almost 50 years ago by Meyer [3] and later by Dozov [4] and experimentally discovered in 2011 [5]. In the *N*_{TB} phase, the local directors form a helix and are tilted with respect to the helical axis, and a striking feature is that the pitch length of the helix is extremely short, typically just a few molecular lengths [6,7]. The formation of chirality by this system of achiral molecules is spontaneous and equal numbers of left- and right-handed helices are

CONTACT Rebecca Walker  rebecca.walker@abdn.ac.uk

 Supplemental data for this article can be accessed online at <https://doi.org/10.1080/02678292.2024.2334342>.

© 2024 The Author(s). Published by Informa UK Limited, trading as Taylor & Francis Group.

This is an Open Access article distributed under the terms of the Creative Commons Attribution-NonCommercial-NoDerivatives License (<http://creativecommons.org/licenses/by-nc-nd/4.0/>), which permits non-commercial re-use, distribution, and reproduction in any medium, provided the original work is properly cited, and is not altered, transformed, or built upon in any way. The terms on which this article has been published allow the posting of the Accepted Manuscript in a repository by the author(s) or with their consent.

obtained. This double degeneracy may be removed, however, either by the addition of a chiral dopant [8] or if the dimers themselves are chiral [9,10], and the chiral N_{TB}^* phase is observed. The central premise of Dozov's seminal work is that bent molecules have a natural tendency to pack into bent structures, but given that pure bend cannot efficiently fill space, it must be accompanied by other local deformations of the director, namely twist or splay [4]. In the case of twist, the twist-bend nematic phase is formed. Thus, within the framework of Dozov's model molecular bend is a prerequisite to the formation of the N_{TB} phase, and this has been borne out experimentally [11,12]. We note that recently an even-membered dimer was reported to exhibit the N_{TB} phase, but this contained a disulphide link in the spacer ensuring the dimer was bent, although technically even-membered [13].

Using these symmetry arguments, Dozov also predicted the formation of heliconical smectic phases (SmC_{TB}) by achiral bent molecules [4], and these have now been found experimentally for odd-membered nonsymmetric dimers in which two different mesogenic units are linked by the spacer [14,15]. We have shown the existence of three different variants of the SmC_{TB} phase: the $SmC_{TB-\alpha}$, SmC_{TB-SH} and SmC_{TB-DH} phases [2]. In each, the director describes a helix, and is tilted with respect to the smectic layer normal that lies along the helical axis. In the $SmC_{TB-\alpha}$ phase, the pitch length is incommensurate with the layer spacing, whereas in the SmC_{TB-SH} phase, the pitch length corresponds to four molecular layers. In the SmC_{TB-DH} phase, a secondary longer helix is superimposed on the short, four-layer basic unit of the SmC_{TB-SH} phase [2,16]. The secondary helix is thought to arise from competing tendencies to form four-layer and bilayer structures.

Our knowledge of the heliconical smectic phases derives almost entirely from the study of odd-membered liquid crystal dimers in which two differing mesogenic units are connected *via* the flexible spacer [15–19]. From a molecular design viewpoint, this architecture was adopted because it allows for the control of structure by modifying the interaction between the two differing mesogenic units, and if one of these possesses a terminal chain, then varying chain length provides control over molecular inhomogeneity, an important factor driving microphase segregation known to promote smectic behaviour [20]. The general family of compounds, the 1-(4-cyanobiphenyl-4'-yl)- ω -(4-alkylanilinebenzylidene-4'-oxy)alkanes (Figure 1), have proven to be a rich source of twist-bend liquid crystal phases [16,19]. The acronym used to refer to these compounds is $CBnO.m$ in which CB refers to the

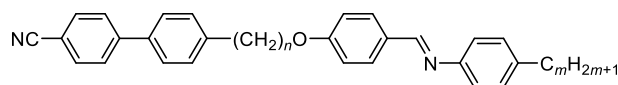


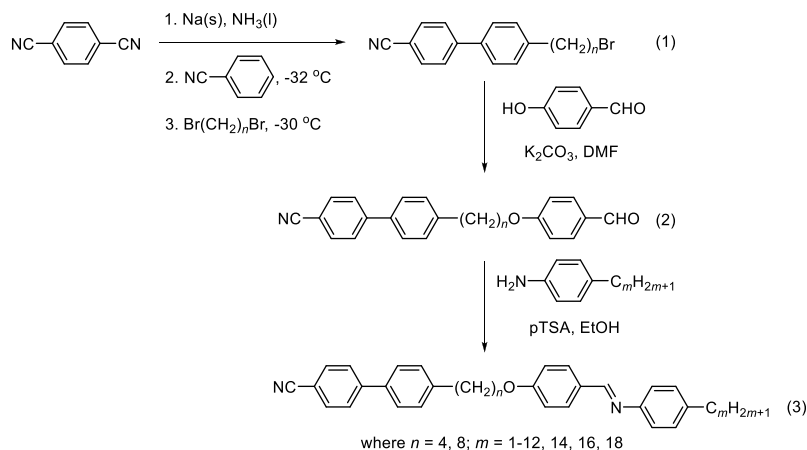
Figure 1. The molecular structure of the 1-(4-cyanobiphenyl-4'-yl)- ω -(4-alkylanilinebenzylidene-4'-oxy)alkanes ($CBnO.m$).

cyanobiphenyl unit, the period to the benzylideneaniline fragment, O to the ether link, and n and m indicate the number of carbon atoms in the spacer and terminal chain, respectively. We have previously reported the liquid crystalline properties of the $CB6O.m$ [19] and $CB10O.m$ series [16]. For the $CB6O.m$ series, the N_{TB} phase was observed for $m = 1$ –10 and smectic behaviour emerged for $m \geq 10$ including examples of the SmC_{TB-SH} and SmC_{TB-DH} phases [15,19]. By comparison, for the $CB10O.m$ series, an intercalated smectic C_A phase is observed if $m/11 \approx 0.5$. Either side of this condition, the twist-bend nematic phase is observed, and for $m > 10$, the SmC_{TB-SH} and SmC_{TB-DH} phases are seen [16]. These studies focused on the dependence of phase behaviour on the length of the terminal chain, m , but it is clear that it is the ratio of terminal chain to spacer chain length, m/n , which plays a critical role in determining phase behaviour. Although studies have been undertaken probing the effects of spacer length on the stability of the N_{TB} phase [21–23], we are unaware of any such investigation involving the twist-bend smectic phases. To begin to address this issue, here we directly ask the question, what effect does the spacer length have on the formation of twist-bend smectic phases? Hence, we report the phase behaviour of the $CB4O.m$ and $CB8O.m$ series and compare this with that of the $CB6O.m$ and $CB10O.m$ series to obtain oversight of the dependence of the phase behaviour on spacer length. We note that these series all contain an odd-membered spacer, a structural prerequisite for the observation of the twist-bend phases.

Experimental

Synthesis

The synthetic method used to obtain the $CB4O.m$ and $CB8O.m$ series is shown in Scheme 1 and involves three steps. First, the 4'-(ω -bromoalkyl)-[1,1'-biphenyl]-4-carbonitriles (1) were synthesised using a sodium-mediated aromatic cross-coupling reaction [24,25] and subsequently reacted with 4-hydroxybenzaldehyde in a Williamson ether reaction to give the 4'-(ω -(4-formylphenoxy)alkyl)-[1,1'-biphenyl]-4-carbonitriles (2) [19]. A Schiff's base synthesis with the appropriate n -alkylaniline yielded the desired products (3) [19].



Scheme 1. Synthetic route to the CBrO.*m* dimers.

Full synthetic details and analytical data for products and intermediates can be found in the ESI.

Materials

All reagents and solvents available commercially were purchased from Sigma Aldrich, Alfa Aesar, ACROS Organics, Fluorochem or TCI Chemicals and used as received.

Structure and purity analysis

The proposed structures of all the final products and their intermediates were characterised using a combination of ^1H and ^{13}C NMR, and FTIR spectroscopies. ^1H and ^{13}C NMR spectra were recorded on a 400 MHz Bruker Avance III HD NMR spectrometer. Infrared spectra were recorded on a Perkin Elmer Spectrum Two FTIR spectrometer with an ATR diamond cell. The purities of the final products were verified using C, H, and N microanalysis performed by the Analytical Laboratory in the School of Chemistry at the London Metropolitan University and the University of Strathclyde External CHN Analysis service. High-resolution mass spectrometry was carried out using a Waters XEVO G2 Q-ToF mass spectrometer operated by Dr Morag Douglas at the University of Aberdeen.

Optical studies

Phase characterisation was performed by polarised optical microscopy (POM) using a Zeiss AxioImager A2m microscope equipped with a Linkam T96 heating stage. Samples were sandwiched between glass plates, giving several micrometre-thick films. Selected samples were also prepared in commercial cells purchased from

INSTEC with a cell thickness of 2.9–3.5 μm and treated for planar anchoring.

Measurements of optical birefringence were performed with a set-up based on a photoelastic modulator (PEM-90, Hinds) working at a modulation frequency $f = 50$ kHz; a halogen lamp (Hamamatsu LC8) was used as a light source, equipped with a narrow bandpass filter (532 nm). The signal from a photodiode (FLC Electronics PIN-20) was de-convoluted with a lock-in amplifier (EG&G 7265) into 1f and 2f components to yield a retardation induced by the sample. Knowing the sample thickness, the retardation was recalculated into optical birefringence. Samples were prepared with homogeneous alignment in cells of 1.5 μm thickness purchased from the Warsaw Military University of Technology (WAT).

Differential scanning calorimetry

The phase behaviour of the dimers was studied by differential scanning calorimetry using a Mettler-Toledo DSC1 or DSC3 fitted with an intracooler and calibrated using indium and zinc as standards. Heating and cooling rates were 10 K min^{-1} , and all samples were measured under a nitrogen atmosphere. Transition temperatures and associated enthalpy changes were extracted from the second heating trace unless otherwise noted. For each sample, two aliquots were measured, and the data listed are the average of the two sets of data.

X-ray diffraction

2D diffraction patterns were obtained with the Bruker D8 GADDS system (CuK α radiation, Goebel mirror monochromator, 0.5 mm point beam collimator,

VANTEC2000 area detector), equipped with a modified Linkam heating stage. Samples were prepared as droplets on a heated surface. The temperature dependence of the smectic layer thickness was determined from the small-angle X-ray diffraction experiments performed with the Bruker D8 Discover system (CuK α line, Goebel mirror, Anton Paar DCS350 heating stage, scintillation counter) working in the reflection mode. Homeotropically aligned samples were used and prepared as a thin film on a silicon reflectionless wafer. The small-angle X-ray diffraction (SAXS) patterns for powder samples were obtained with a Bruker Nanostar system using CuK α radiation, and patterns were collected with a VANTEC2000 area detector. The temperature of the samples was controlled with a precision of ± 0.1 K.

Resonant soft X-ray diffraction

Resonant soft X-ray diffraction (RSoXS) studies were performed at the Advanced Light Source, Lawrence Berkeley National Laboratory on the soft X-ray beam

line (11.0.1.2). The energy of the incident beam was tuned to the K-edge of carbon absorption (283 eV). Samples with a thickness lower than 1 μm were placed on a transmission electron microscopy grid. The scattering intensity was recorded using the Princeton PI-MTE CCD detector.

Results and discussion

CB4O.*m* series

The transitional properties of the CB4O.*m* series are listed in Table 1, and the dependence of the transition temperatures on the length of the terminal chain, *m*, is shown in Figure 2(a). The conventional nematic phase (N) was identified by the POM observation of characteristic schlieren (Figure 3(a)) and uniform (Figure 3(c)) optical textures when sandwiched between untreated glass slides and in cells treated for planar alignment and unidirectionally rubbed, respectively. The twist-bend nematic phase (N_{TB}) in homologues *m* = 1–8 was assigned from the change in the schlieren texture of the

Table 1. Phase transition temperatures ($^{\circ}\text{C}$) and associated entropy changes (in parenthesis, scaled by R) for the CB4O.*m* series.

<i>m</i>	Cr-	SmX3	SmC _{TB-DH}	SmC _{TB-SH}	SmA	N_{TB}	N
1	147 (8.54)					80 [†]	113 [†]
2	130 (9.18)					69 [†]	103 [†]
3	112 (9.90)					74 (0.1)*	104 (0.1)
4	108 (10.30)					61 [†]	91 (0.1)
5	95 (8.97)					65 (≈ 0)*	94 (0.1)
6	91 (9.83)					56 (0.1)*	83 (0.1)*
7	85 (10.41)					61 (≈ 0)*	89 (0.1)
8	86 (11.09)					59 (≈ 0)*	83 (0.1)*
9	80 (8.21)		69 (≈ 0)*	74 (0.1)*			90 (0.1)
10	73 (9.55)		66 [†]	79 ^a	79 (0.3) ^a		89 (0.2)
12	85 (12.25)	57 [†]	72 (≈ 0)*	90 (≈ 0)	93 (0.8)		
14	83 (11.09)	56 [†]	75 (≈ 0)*	97 (0.1)	102 (1.3)		
16	91 (16.29)	64 [†]	81 (≈ 0)*	97 (≈ 0)	104 (1.5)		
18	87 (13.24)	64 [†]	76 (≈ 0)*	103 (0.1)	112 (1.9)		

*denotes a temperature obtained from DSC cooling trace.

[†]denotes temperature obtained using POM.

^adenotes peak overlap; quoted entropy encompasses both SmA and SmC_{TB-SH} phases.

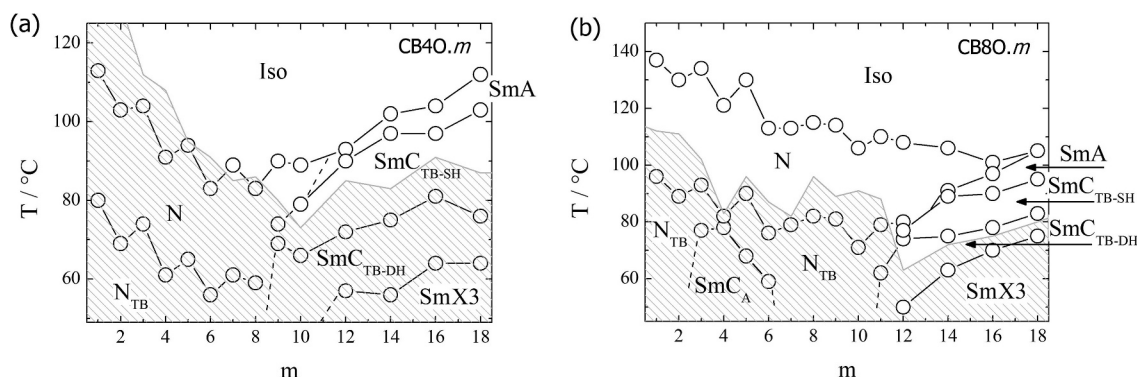


Figure 2. The dependence of the transition temperatures on the length on the terminal chain, *m*, for the (a) CB4O.*m* and (b) CB8O.*m* series. Grey striped areas mark the range of monotropic LC phase behaviour.

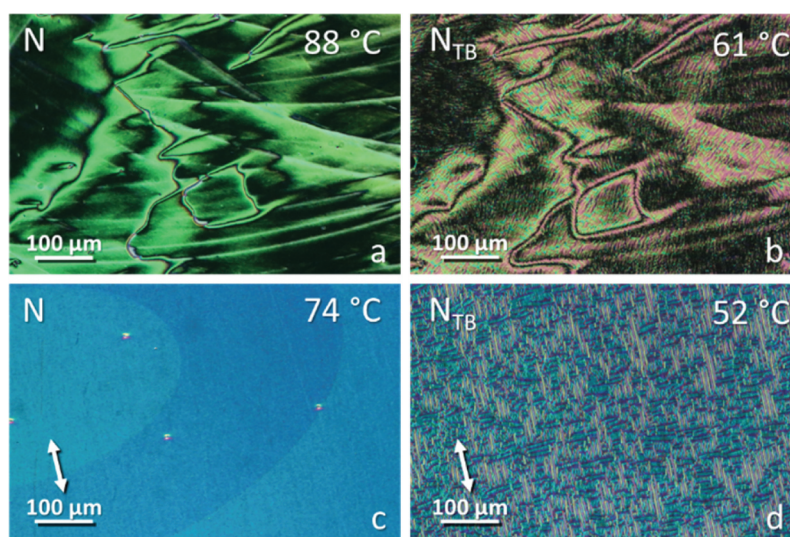


Figure 3. (Colour online) POM textures obtained for CB40.5 in (a) (c) nematic and (b) (d) twist-bend nematic phases in untreated slides (a,b) and cells with planar alignment (c,d).

N phase to a ‘blocky’ schlieren texture (Figure 3(b)), and by the emergence of a striped texture (Figure 3(d)) from the preceding uniform texture of the N phase. In addition, the N– N_{TB} phase transition was marked by the cessation of optical flickering associated with director fluctuations in the nematic phase.

The temperatures of the N_{TB} –N and N–I transitions, T_{NTBN} and T_{NI} , respectively, both decrease on increasing m and superimposed upon this is a weak odd – even effect in which the odd members show the higher values. The underlying decreasing trend in both T_{NTBN} and T_{NI} on increasing m presumably reflects the dilution of the interactions between the mesogenic units on increasing the volume fraction of alkyl chains, and

the odd-even effect may be attributed to the dependence of molecular shape on the parity of the terminal chain as described in detail elsewhere [19]. Rapid crystallisation of the N_{TB} phase precluded further investigation of the shorter homologues $m = 1$ –8.

For $m = 9$ and 10, the N_{TB} phase is extinguished. On cooling the N phase of $m = 9$ two heliconical smectic phases, SmC_{TB-SH} and SmC_{TB-DH} , are observed, exhibiting biaxial and uniaxial optical properties, respectively. In areas with homeotropic alignment, the SmC_{TB-SH} phase showed a dynamic schlieren-like pattern with areas of distinct stripes of alternating birefringence, while for the SmC_{TB-DH} phase, a uniformly black texture was found, see Figure 4. For $m = 10$, a phase sequence of N–SmA– SmC_{TB-SH} – SmC_{TB-DH} is observed. For all

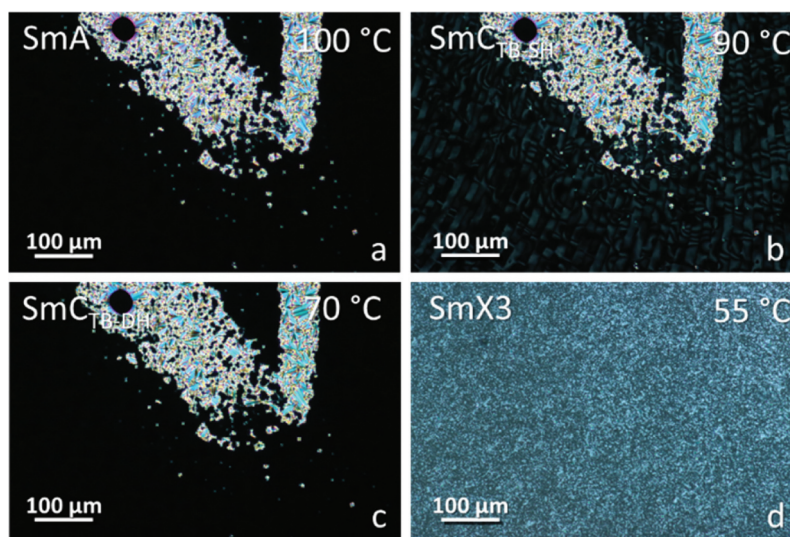


Figure 4. (Colour online) POM textures obtained for CB40.14 in (a) smectic A, (b) smectic C_{TB-SH} , (c) smectic C_{TB-DH} and (d) smectic X3 phases in untreated slides.

smectic phases XRD studies revealed a lamellar structure, with layer spacing, d , being almost twice the molecular length, L ; $d/L \sim 1.8$ (Figure S3). This partially bilayer, interdigitated structure is obtained by antiparallel arrangement of cyanobiphenyl moieties of molecules from neighbouring molecular layers. The nematic-smectic phase transition is accompanied by a slight increase in the birefringence arising from an increase in the orientational order parameter associated with layer formation (see Figure 5). The onset of the $\text{SmC}_{\text{TB-SH}}$ phase is accompanied by a gradual decrease in the birefringence due to the tilting of the molecules. Transition from the biaxial $\text{SmC}_{\text{TB-SH}}$ phase to the uniaxial $\text{SmC}_{\text{TB-DH}}$ phase causes a step-like increase in the measured birefringence for planar cells with a book-shelf geometry in which the molecules in the $\text{SmC}_{\text{TB-SH}}$ phase are preferentially tilted in the sample plane, whereas in the $\text{SmC}_{\text{TB-DH}}$ phase, the additional helix causes the full averaging of the molecular positions on the tilt cone [16].

For $m \geq 11$, the conventional nematic phase is extinguished and on cooling the isotropic phase the SmA phase is formed, followed by the SmC_{TB} phases. Following the underlying decreasing trend in both T_{NTBN} and T_{NI} on increasing m , this is reversed at $m = 9$ and the clearing temperature subsequently increases with m . This change in behaviour is accompanied by the switch from an intercalated to an interdigitated packing of the molecules and subsequent emergence of a SmA-I transition. The formation of the interdigitated SmA phase is presumably driven by the antiparallel association of the polar and polarisable cyanobiphenyl units to minimise the dipolar energy and arises due the molecular inhomogeneity associated with

the long terminal chain. We will return to a discussion of this behaviour later.

For $m = 12, 14, 16$ and 18 on cooling the $\text{SmC}_{\text{TB-DH}}$ phase another lamellar phase, arbitrarily denoted SmX3 , was found, characterised by increased positional order of the molecules within the smectic layers. The layer spacing (see Figure S3) was found to monotonically increase on cooling through the $\text{SmA-SmC}_{\text{TB-SH-SmC}_{\text{TB-DH}}$ phase sequence, and sharply increase on moving to the SmX3 phase, consistent with an increase in the order parameter. It is likely this phase is the same as the higher-order phase found at temperatures below the $\text{SmC}_{\text{TB-DH}}$ phase for the CB10O.m series in homologues with $m > 12$ [16].

The heliconical character of both SmC_{TB} phases was confirmed by resonant X-ray scattering studies performed for homologue CB4O.12 (Figure 6). In the $\text{SmC}_{\text{TB-SH}}$ phase, a single diffraction signal corresponding to twice the periodicity of the smectic layers (four molecular lengths) was recorded, and a basic repeating unit is composed of four molecular layers in which changes of the azimuthal direction of the director are defined by a distorted clock model [15,16]. At the transition to the $\text{SmC}_{\text{TB-DH}}$ phase, this signal splits symmetrically into two branches indicating the formation of a secondary helix [15,16]. The splitting of the signal is discontinuous, evidencing the first-order character of the $\text{SmC}_{\text{TB-SH-SmC}_{\text{TB-DH}}$ phase transition. The non-equal intensities of the two branches are consistent with the distortion of the four-layer clock unit, over which the longer helix is superimposed. Moreover, an additional diffraction signal appears at low angles, corresponding to half the pitch length of the secondary helix; its temperature evolution shows that on cooling the pitch decreases from 70 nm to 35 nm.

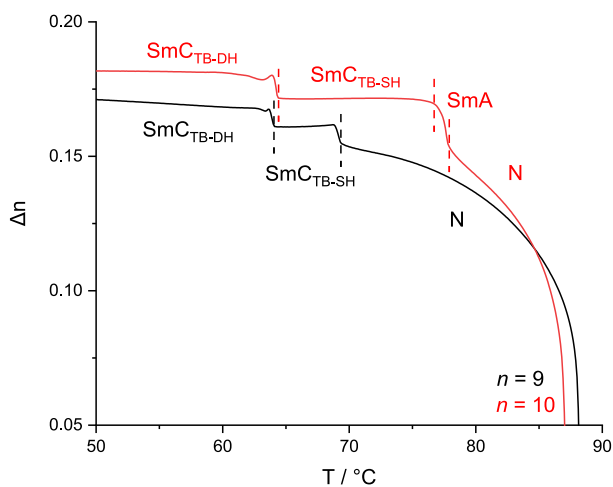


Figure 5. (Colour online) Optical birefringence as a function of temperature for CB40.9 (black line) and CB40.10 (red line).

CB8O.m series

We now turn our attention to the series with a longer odd-membered spacer, the CB8O.m series. Table 2 lists the transitional properties of the series, and the dependence of the transition temperatures on the length of the terminal chain m is shown in Figure 2(b). All 15 homologues show an enantiotropic conventional nematic phase, and for $m = 1-12$ an N_{TB} phase was also seen. These were assigned based on the observation of characteristic optical textures described earlier, and representative examples are shown in Figure 7. The temperature dependence of the optical birefringence, shown in Figure S1 for CB8O.5 , reveals a small jump in Δn at T_{NTBN} , which is thought to reflect the increase in the order parameter associated

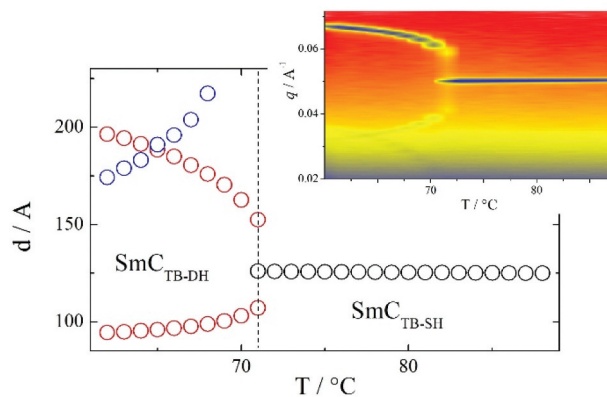


Figure 6. (Colour online) Periodicities corresponding to diffraction signals recorded under resonance condition for CB40.12, the inset shows the temperature evolution of the RSoXS signals.

with the weakly first-order N–N_{TB} transition [26]. On further cooling, the optical birefringence gradually decreases due to the tilting of the molecules with respect to the helical axis in the N_{TB} phase. X-ray diffraction patterns obtained for both nematic phases consist of weak, broad signals indicative of a liquid-like arrangement of the molecules.

For $m = 3$ –6, an anticlinic SmC_A phase is observed at temperatures below the N_{TB} phase. This was assigned based on the development of a focal conic fan texture, and a somewhat mobile schlieren texture formed on shearing the sample (Figure 7(c,d)). The X-ray diffraction patterns obtained for the N_{TB} and SmC_A phases exhibited by CB8O.3 are shown in Figure 8. The small-angle signal is broad in the N_{TB} phase due to the liquid-like positional ordering of the molecules and narrows to the machine-resolution limit in the SmC_A phase with the development of a periodic, lamellar structure. The broad wide-angle reflection confirms a liquid-like in-plane ordering of the

molecules in the SmC_A phase. The ratio of the layer spacing to molecular length in the SmC_A phase is approximately 0.5 indicating an intercalated arrangement of the molecules. The formation of the SmC_A phase is driven by the favourable specific interaction between the unlike mesogenic groups and this is described in detail elsewhere [2]. The N_{TB}–SmC_A phase transition is again accompanied by a sharp increase in the birefringence arising from an increase in the orientational order parameter associated with layer formation (Figure S1). On cooling the SmC_A phase of CB8O.3, CB8O.4 and CB8O.6, the schlieren texture becomes smoother and the defect lines become more diffuse (Figure 7(e)), and a scratched line pattern develops across this texture on further cooling the former two homologues (Figure 7(f)). X-ray diffraction patterns of these two low-temperature phases show a narrowing, and subsequently a splitting of the high angle signal, suggesting an increase in order within the smectic layers (Figure S4). This behaviour is in line with that observed previously for CB8O.4 [27]: the higher temperature phase has therefore been assigned as a higher-order hexatic-type phase and the lower temperature phase as a soft-crystal-type phase, arbitrarily designated as SmX1 and SmX2, respectively.

Smectic behaviour is absent for homologues $m = 7$ –10, but re-emerges at $m = 11$. This trend was reported also for the CB10O. m series [16], and attributed to the destabilisation of intercalated lamellar packing as the terminal chain length increases. Despite a thermal transition evident at 61°C in the DSC cooling trace for CB8O.11, phases either side of this transition exhibited a rope-like texture when viewed in cells treated for planar alignment and a pseudo-isotropic texture in cells with homeotropic anchoring. This strongly suggests the formation of the heliconical SmC_{TB-DH} phase

Table 2. Phase transition temperatures (°C) and associated entropy changes (in parenthesis, scaled by R) for the CB8O. m series.

m	Cr-	SmX3	SmX2	SmX1	SmC _{TB-DH}	SmC _{TB-SH}	SmA	SmC	N _{TB}	N
1	112 (9.4)								96 (≈0)*	137 (0.3)
2	111 (7.7)								89(≈0)*	130 (0.4)
3	102 (8.3)		32 [†]	73 (0.6)*				77 (0.7)*	93 (≈0)*	134 (0.3)
4	83 (3.7)		25 [†]	64 (0.6)*				78 (0.6)*	82 (≈0)*	121 (0.3)
5	96 (6.6)							68 [†]	90 (≈0)*	130 (0.2)
6	87 (17.4)			53 [†]				59 [†]	76 (≈0)*	113 (0.3)
7	82 (16.8)								79 (≈0)*	113 (0.5)
8	96 (19.7)								82 [†]	115 (0.3)
9	89 (18.7)								81 (≈0)*	114 (0.3)
10	91 (12.9)								71 (0.1)*	106 (0.3)
11	88 (16.4)				61(≈0)*				97 (≈0)	110 (0.2)
12	63 (9.7)	50 (1.5)*			74 [†]	78 [†]			80 [†]	108 (0.3)
14	72 (16.4)	63 (2.0)*			75 [†]	89 [†]	91 [†]			106 (0.3)
16	75 (16.9)	70 (2.7)*			78 (≈0)	90 (0.1)	97			101 (0.2)
18	80 (21.1)	75 (3.3)*			83 (≈0)	95 (0.1)	105 (0.9)			105 [†]

*denotes a temperature obtained from DSC cooling trace.

[†]denotes temperature obtained using POM.

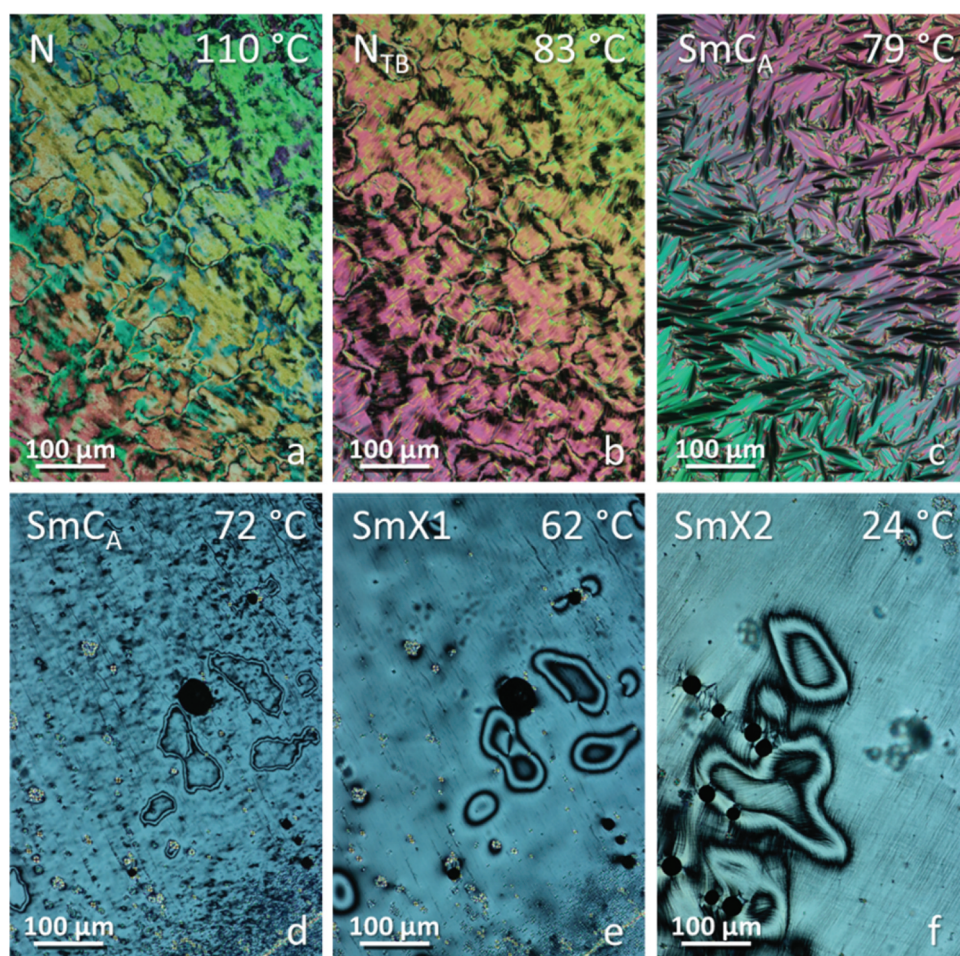


Figure 7. (Colour online) POM textures obtained for CB80.4 in (a) nematic, (b) twist-bend nematic, (c) (d) smectic C_A before and after mechanical shear, respectively, (e) SmX1 and (f) SmX2 phases.

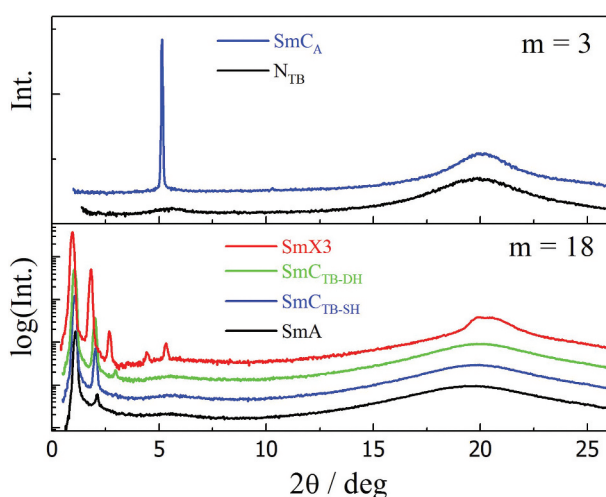


Figure 8. (Colour online) X-ray diffraction patterns for CB80.3 and CB80.18.

directly below the N_{TB} phase [19]. The lamellar nature of the lower-temperature phase is confirmed by the observation of a sharp small-angle signal in the X-ray

diffraction pattern (Figure S5). The N_{TB} phase is extinguished for $m > 12$, and for the longer homologues a sequence of up to four smectic phases was observed. The highest temperature of these is the orthogonal SmA phase, and at lower temperatures, two tilted, heliconical phases are formed, SmC_{TB-SH} and SmC_{TB-DH} . The texture of the SmC_{TB-SH} phase is again a dynamic schlieren-like pattern with areas of distinct stripes of alternating birefringence, which is extinguished upon transition to the optically uniaxial SmC_{TB-DH} phase. Optical birefringence behaves as described earlier for the long homologues of the CB4O. m series, see Figure S2. The X-ray diffraction patterns for the SmA and SmC_{TB} phases (shown for CB80.18 in Figure 8) are essentially identical and consist of sharp small angle and diffuse wide-angle signals reflecting the liquid-like arrangement of the molecules within the smectic layers. The small-angle signal appears at approximately twice the molecular length, indicating a bilayer arrangement of molecules within the layers. In the lowest temperature smectic phase, the wide-angle signal narrows and

higher harmonics of the small-angle signal develop, indicating a higher ordered phase. Owing to similarities between POM textures and X-ray patterns for this phase and those reported for CB4O.*m* (as SmX3, see earlier) and CB10O.*m* (as SmY) [16], we suggest that this is the same phase in all series and assign it here again as SmX3.

CB6O.*m* and CB10O.*m*

The CB6O.*m* [19] and CB10O.*m* series [16] also show a change in molecular packing on increasing the terminal chain length, from intercalated arrangements for short terminal chains (for the CB6O.*m* series only nematic phases are found whereas for the CB10O.*m* series, a SmC_A phase is also observed) through to a bilayer structure for the long homologues (Figure 9). For CB6O.*m*, the crossover from intercalated to interdigitated packing lies between *m* = 9 and 10 and for the CB10O.*m* series between *m* = 11 and 12. In both series, the longer homologues form helical tilted smectic phases on cooling either nematic or SmA phases.

Comparison of the CB*n*O.*m* series

Figure 10 compares the transition temperatures shown by the four CB*n*O.*m* series. The CB4O.*m* compounds show the lowest values of *T*_{NI} for any given value of *m* (Figure 10(a)). On increasing *n*, *T*_{NI} increases passing to the CB6O.*m* series and again to the CB8O.*m* and CB10O.*m* series for which the values of *T*_{NI} are rather similar. This reflects rather typical behaviour for a series of nematogenic dimers in which the length of the flexible spacer, *n*, is varied [22,23]. Thus, for a given series of dimers, the values of *T*_{NI} for the even members tend to fall on increasing *n*, whereas those of the odd members initially increase on increasing *n*, pass through

a maximum value and then slowly decrease. The decrease in *T*_{NI} seen for the even members is associated with the dilution of the interactions between the mesogenic units arising from the increased volume fraction of alkyl chains within the system. For the odd members, however, the initial increase in *T*_{NI} on increasing *n* reflects the increase in molecular flexibility which allows for more linear conformations of the spacer to be explored. At some point, this effect is offset by the increasing dilution of the interactions between the mesogenic units and a maximum value of *T*_{NI} is reached, and further increases in spacer lengths see the dilution factor dominate and *T*_{NI} falls.

The values of *T*_{NTBN} show the same trend on increasing *n* as seen for *T*_{NI} (Figure 10(b)). It may appear counter-intuitive that the values of *T*_{NTBN} are lowest for the most bent dimers, *i.e.* those having the shortest spacer length, *n* = 4, compared to those of the corresponding members of the series having longer spacers. This indicates that the stability of the N_{TB} phase is not entirely associated with molecular curvature. Instead, the reduction in molecular curvature on moving to longer spacers is counteracted by the corresponding increase in molecular flexibility that facilitates enhanced interactions between the mesogenic groups, and increases not only *T*_{NI} but also *T*_{NTBN}.

Figure 10(d) compares the upper temperature limits of the interdigitated SmA phase stability, *i.e.* SmA-I or SmA-N transition temperatures. It is striking, however, that the trends observed for *T*_{NI} and *T*_{NTBN} are now reversed. Indeed, the value of *T*_{NI} for CB4O.1 is considerably lower than that of the other CB*n*O.1 compounds, whereas *T*_{SmAI} for CB4O.18 is the highest among all CB*n*O.18 homologues. This strongly suggests that molecular curvature is less important in determining the stability of the interdigitated SmA phase. Instead, the greater

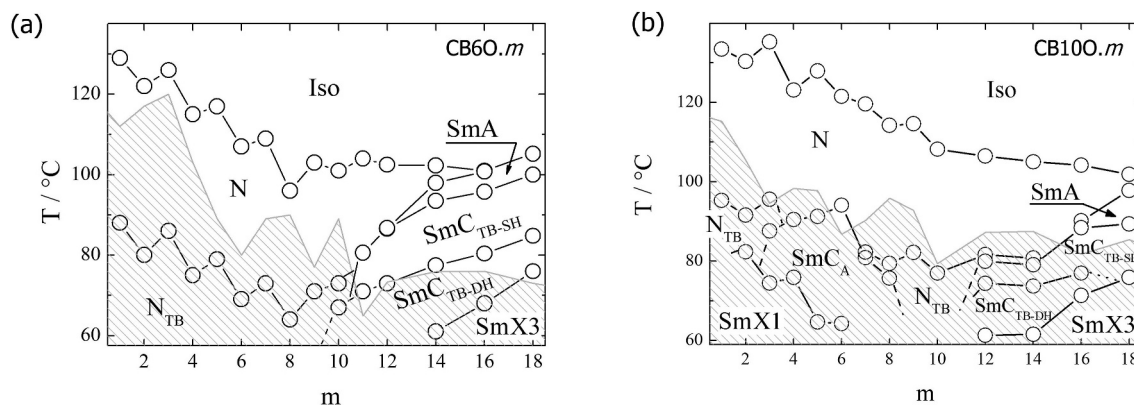


Figure 9. The dependence of the transition temperatures on the length on the terminal chain, *m*, for the (a) CB6O.*m* and (b) CB10O.*m* series. Grey striped area marks the monotropic range of the mesophases.

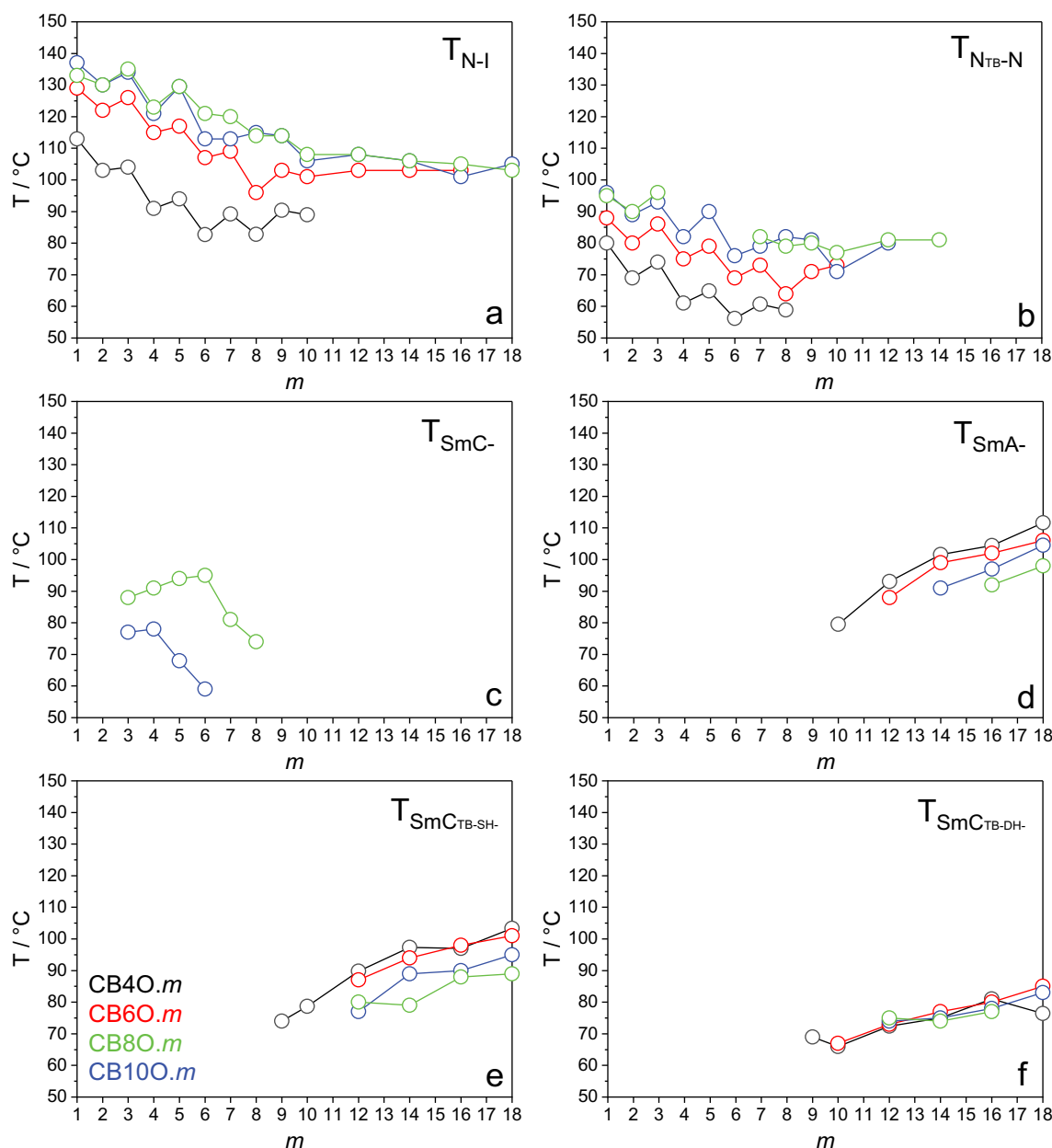


Figure 10. (Colour online) A comparison of the phase transition temperatures for CB_{*n*}O.*m* series, where *n* = 4, 6, 8, 10 and *m* = 1–10, 12, 14, 16, 18.

molecular inhomogeneity arising from the shorter spacer length for any given value of *m* stabilises the separation of unlike molecular fragments in the smectic phase.

We can now explore the role of the spacer chain length in governing the molecular packing seen for the CB_{*n*}O.*m* dimers. For all four series, intercalated packing is shown by short terminal chain lengths, and interdigitated/bilayer arrangements for longer homologues. The length of the spacer, *n*, determines the ‘crossover’ point between these packing types; increasing *n* from 4 to 10 moves the crossover from *m* = 8 to *m* = 12. The short homologues in

both the CB4O.*m* and CB6O.*m* series form only nematic phases, and increasing spacer length gives rise to intercalated SmC_A phases in the CB8O.*m* and CB10O.*m* series, and higher values of T_{SmCAN} are observed for the latter (Figure 10(c)). In each series, helical smectic phases are observed for the longer homologues in which the layer spacing corresponds to around two molecular lengths.

The intercalated packing observed for the shorter terminal chain homologues of all four series is thought to be driven by a favourable specific interaction between the unlike mesogenic units, suggested to be an electrostatic quadrupolar interaction between groups having

quadrupole moments of opposite signs [28]. In this arrangement, the terminal chain must be accommodated in the void space determined by the length of the spacer. For all four series, the members with the shortest terminal chains show N and N_{TB} phases in which the local periodicity measured along the director corresponds to half the molecular length, suggesting that dynamic associations between the unlike mesogenic units give rise to short-range intercalated arrangements but that the terminal chain is too short to fill space effectively to stabilise a smectic phase. We note, however, that CBO12O.2 does exhibit intercalated smectic phase behaviour and has an even more pronounced mismatch in spacer and terminal chain lengths [27,29] but the bent shape of the odd-membered dimers reported here further destabilises lamellar packing. Increasing the terminal chain lengths for the members of the CB8O.*m* and CB10O.*m* series such that the ratio *n:m* is around two sees the emergence of the intercalated SmC_A phase. This condition maximises the packing efficiency in the intercalated arrangement. The SmC_A-N transition temperature is around 20 K higher for the CB10O.*m* series than for the corresponding member of the CB8O.*m* series, reflecting the increasing ease of accommodating a terminal chain in the intercalated structure on increasing *n*. Increasing the terminal chain further in the CB8O.*m* and CB10O.*m* series sees the SmC_A phase extinguished and a return to exclusively nematic behaviour in which, again the periodicity along the director corresponds to approximately half the molecular length. This indicates that although the favourable interactions between the unlike mesogenic units drive local intercalated associations between the dimers, the longer terminal chains cannot be accommodated which destabilises lamellar packing. At some point, the terminal chains become too long and disrupt the dynamic associations between the unlike mesogenic groups and instead we see interdigitated molecular associations driven by the anti-parallel arrangement of the polar and polarisable cyanobiphenyl units. As would be expected, this switch-over in behaviour shifts to higher values of *m* as the spacer length is increased. It is notable that for the CB4O.*m* series this switch from intercalated to interdigitated packing is associated with the onset of an increasing trend in the clearing temperature (Figure 2) reflecting the enhanced interactions between the mesogenic units in the latter arrangement.

We now turn our attention to the heliconical SmC_{TB-SH} and SmC_{TB-DH} phases. The upper temperature stability limit of the SmC_{TB-SH} phase (Figure 10(e)) follows the same trend seen for the interdigitated smectic A phase (Figure 10(d)), whereas the stability of the SmC_{TB-DH} phase appears rather insensitive to spacer length

(Figure 10(f)). The former observation suggests the importance of molecular inhomogeneity on the formation of the SmC_{TB-SH} phase, although alternatively may reflect differences in bend elastic constants arising from molecular shape [30].

Finally, we note that these heliconical smectic phases appear not to be compatible with intercalated packing of the dimers. This may be related to the elastic constants for the intercalated SmC_A phase and its network structure. ²H-NMR spectroscopic studies revealed that the intercalated smectic phase shown by CBO11O.10-d₂ is considerably more viscous than the interdigitated (bilayer) SmA phase of CBO5O.10-d₂ at the same absolute temperature and essentially the same shifted temperature [31]. This was attributed to the network structure of the intercalated smectic phase.

Conclusions

This study of four series of the CB*n*O.*m* family of dimers has reinforced the observation that the nature of the local packing of the molecules depends on the *n:m* ratio. For ratios around two and higher, intercalated packing is favoured and driven by a specific, favourable interaction between the unlike mesogenic units. For the longer spacers studied, *n* = 8 and 10, the intercalated SmC_A was observed. Increasing the terminal chain length (decreasing the *n:m* ratio) destabilises intercalated packing and a switch to interdigitated bilayer arrangements is observed. This is driven by the antiparallel association of the cyanobiphenyl units, and interdigitated smectic phases are thought to arise due to the enhanced molecular inhomogeneity. Heliconical SmC_{TB-SH} and SmC_{TB-DH} phases are observed only for interdigitated packing arrangements. The absence of intercalated heliconical smectic phases is attributed to the high viscosity associated with the network structure of the intercalated smectic phase. The generality of these observations must now be tested.

Acknowledgments

A. F. A. wishes to thank the Ministry of Education and the University of Hail, Saudi Arabia, through the Cultural Bureau of Saudi Arabia, London, for their financial support during the study period. The research was supported by the National Science Centre (Poland) under grant no. 2021/43/B/ST5/00240. The beamline 11.0.1.2 at the Advanced Light Source at the Lawrence Berkeley National Laboratory is supported by the Director of the Office of Science, Office of Basic Energy Sciences, of the U.S. Department of Energy under Contract No. DE-AC02-05CH11231.

Disclosure statement

No potential conflict of interest was reported by the author(s).

Funding

The work was supported by the Narodowym Centrum Nauki [2021/43/B/ST5/00240]; Saudi Arabia Cultural Bureau in London.

ORCID

Ahlam F Alshammari  <http://orcid.org/0000-0002-6647-2196>

Ewan Cruickshank  <http://orcid.org/0000-0002-4670-8405>
Magdalena Majewska  <http://orcid.org/0000-0001-9395-6834>

Damian Pocięcha  <http://orcid.org/0000-0001-7734-3181>

John MD Storey  <http://orcid.org/0000-0002-5261-5467>

Ewa Gorecka  <http://orcid.org/0000-0002-8076-5489>

Corrie T. Imrie  <http://orcid.org/0000-0001-6497-5243>

Rebecca Walker  <http://orcid.org/0000-0001-5167-7183>

References

- [1] Imrie CT, Henderson PA. Liquid crystal dimers and higher oligomers: between monomers and polymers. *Chem Soc Rev.* 2007;36(12):2096–2124. doi: 10.1039/b714102e
- [2] Imrie CT, Walker R, Storey JMD, et al. Liquid crystal dimers and smectic phases from the intercalated to the twist-bend. *Crystals.* 2022;12(9):1245. doi: 10.3390/cryst12091245
- [3] Meyer RB. Les Houches summer school in theoretical physics. In: Balian RG, Weil G, editors. New York (NY): Gordon and Breach; 1976. p. 273–373.
- [4] Dozov I. On the spontaneous symmetry breaking in the mesophases of achiral banana-shaped molecules. *Europhys Lett.* 2001;56(2):247–253. doi: 10.1209/epl/i2001-00513-x
- [5] Cestari M, Diez-Berart S, Dunmur DA, et al. Phase behavior and properties of the liquid-crystal dimer 1',7''-bis(4-cyanobiphenyl-4'-yl) heptane: a twist-bend nematic liquid crystal. *Phys Rev E.* 2011;84:031704. doi: 10.1103/PhysRevE.84.031704
- [6] Borshch V, Kim YK, Xiang J, et al. Nematic twist-bend phase with nanoscale modulation of molecular orientation. *Nat Commun.* 2012;4:2635. doi: 10.1038/ncomms3635
- [7] Chen D, Porada JH, Hooper JB, et al. Chiral heliconical ground state of nanoscale pitch in a nematic liquid crystal of achiral molecular dimers. *Proc Natl Acad Sci USA.* 2013;110:15931–15936. doi: 10.1073/pnas.1314654110
- [8] Archbold CT, Davis EJ, Mandle RJ, et al. Chiral dopants and the twist-bend nematic phase-induction of novel mesomorphic behaviour in an apolar bimesogen. *Soft Matter.* 2015;11:7547–7557. doi: 10.1039/C5SM01935D
- [9] Walker R, Storey JMD, Imrie CT, et al. The chiral twist-bend nematic phase (N*TB). *Chem A Eur J.* 2019;25:13329–13335. doi: 10.1002/chem.201903014
- [10] Walker R, Pocięcha D, Salamoneczyk M, et al. Intrinsically chiral twist-bend Nematogens: interplay of molecular and structural chirality in the NTB phase. *Chemphyschem.* 2023;24(6):e202200807. doi: 10.1002/cphc.202200807
- [11] Mandle RJ. A Ten-year perspective on twist-bend nematic materials. *Molecules.* 2022;27(9):2689. doi: 10.3390/molecules27092689
- [12] Walker R. The twist-bend phases: structure–property relationships, chirality and hydrogen-bonding. *Liq Cryst Today.* 2020;29(1):2–14. doi: 10.1080/1358314X.2020.1771841
- [13] Tufaha N, Gibb CJ, Storey JMD, et al. Can even-membered liquid crystal dimers exhibit the twist-bend nematic phase? The preparation and properties of disulphide and thioether linked dimers. *Liq Cryst.* 2023;50(7–10):1362–1374. doi: 10.1080/02678292.2023.2242824
- [14] Abberley JP, Killah R, Walker R, et al. Heliconical smectic phases formed by achiral molecules. *Nat Commun.* 2018;9(1):228. doi: 10.1038/s41467-017-02626-6
- [15] Salamoneczyk M, Vaupotič N, Pocięcha D, et al. Multi-level chirality in liquid crystals formed by achiral molecules. *Nat Commun.* 2019;10(1):1922. doi: 10.1038/s41467-019-09862-y
- [16] Alshammari AF, Pocięcha D, Walker R, et al. New patterns of twist-bend liquid crystal phase behaviour: the synthesis and characterisation of the 1-(4-cyanobiphenyl-4'-yl)-10-(4-alkylaniline-benzylidene-4'-oxy) decanes (CB10O.m). *Soft Matter.* 2022;18(25):4679–4688. doi: 10.1039/D2SM00162D
- [17] Pocięcha D, Vaupotič N, Majewska M, et al. Photonic bandgap in achiral liquid crystals—A twist on a twist. *Adv Mater.* 2021;33(39):2103288. doi: 10.1002/adma.202103288
- [18] Cruickshank E, Walker R, Strachan GJ, et al. The influence of the imine bond direction on the phase behaviour of symmetric and non-symmetric liquid crystal dimers. *J Mol Liq.* 2023;391:123226. doi: 10.1016/j.molliq.2023.123226
- [19] Walker R, Pocięcha D, Strachan GJ, et al. Molecular curvature, specific intermolecular interactions and the twist-bend nematic phase: the synthesis and characterisation of the 1-(4-cyanobiphenyl-4'-yl)-6-(4-alkylanilinebenzylidene-4'-oxy)hexanes (CB6O.m). *Soft Matter.* 2019;15(15):3188–3197. doi: 10.1039/C9SM00026G
- [20] Imrie CT. Non-symmetric liquid crystal dimers: how to make molecules intercalate. *Liq Cryst.* 2006;33(11–12):1449–1485. doi: 10.1080/02678290601140498
- [21] Forsyth E, Paterson DA, Cruickshank E, et al. Liquid crystal dimers and the twist-bend nematic phase: on the role of spacers and terminal alkyl chains. *J Mol Liq.* 2020;320:114391. doi: 10.1016/j.molliq.2020.114391
- [22] Paterson DA, Abberley JP, Harrison WTA, et al. Cyanobiphenyl-based liquid crystal dimers and the twist-bend nematic phase. *Liq Cryst.* 2017;44:127–146. doi: 10.1080/02678292.2016.1274293

- [23] Paterson DA, Walker R, Storey JMD, et al. Molecular structure and the twist-bend nematic phase: the role of spacer length in liquid crystal dimers. *Liq Cryst.* **2023**;50(4):725–736. doi: [10.1080/02678292.2023.2198505](https://doi.org/10.1080/02678292.2023.2198505)
- [24] Gibb CJ, Storey JMD, Imrie CT. A convenient one-pot synthesis, and characterisation of the ω -bromo-1-(4-cyanobiphenyl-4'-yl) alkanes (CBnBr). *Liq Cryst.* **2022**;49(12):1706–1716. doi: [10.1080/02678292.2022.2084568](https://doi.org/10.1080/02678292.2022.2084568)
- [25] Peshkov RY, Panteleeva EV, Chunyan W, et al. One-pot synthesis of 4'-alkyl-4-cyanobiaryls on the basis of the terephthalonitrile dianion and neutral aromatic nitrile cross-coupling. *Beilstein J Org Chem.* **2016**;12:1577–1584. doi: [10.3762/bjoc.12.153](https://doi.org/10.3762/bjoc.12.153)
- [26] Pocięcha D, Crawford CA, Paterson DA, et al. Critical behavior of the optical birefringence at the nematic to twist-bend nematic phase transition. *Phys Rev E.* **2018**;98:052706. doi: [10.1103/PhysRevE.98.052706](https://doi.org/10.1103/PhysRevE.98.052706)
- [27] Walker R, Pocięcha D, Faidutti C, et al. Remarkable stabilisation of the intercalated smectic phases of nonsymmetric dimers by tert-butyl groups. *Liq Cryst.* **2022**;49(7–9):969–981. doi: [10.1080/02678292.2022.2055797](https://doi.org/10.1080/02678292.2022.2055797)
- [28] Blatch AE, Fletcher ID, Luckhurst GR. The intercalated smectic a phase. The liquid crystal properties of the α -(4-cyanobiphenyl-4'-yloxy)- ω -(4-alkyloxycinnamate)alkanes. *Liq Cryst.* **1995**;18(5):801–809. doi: [10.1080/02678299508036693](https://doi.org/10.1080/02678299508036693)
- [29] Attard GS, Date RW, Imrie CT, et al. Non-symmetric dimeric liquid crystals the preparation and properties of the α -(4-cyanobiphenyl-4'-yloxy)- ω -(4-n-alkylanilinebenzylidene-4'-oxy)alkanes. *Liq Cryst.* **1994**;16(4):529–581. doi: [10.1080/02678299408036531](https://doi.org/10.1080/02678299408036531)
- [30] Cestari M, Frezza E, Ferrarini A, et al. Crucial role of molecular curvature for the bend elastic and flexoelectric properties of liquid crystals: mesogenic dimers as a case study. *J Mater Chem.* **2011**;21(33):12303–12308. doi: [10.1039/c1jm12233a](https://doi.org/10.1039/c1jm12233a)
- [31] Le Masurier PJ, Luckhurst GR. On the molecular organisation in the intercalated smectic a phases formed by the non-symmetric α -(4-cyanobiphenyl-4'-yloxy)- ω -(4-alkylanilinebenzylidene-4'-oxy)alkane dimers. *Chem Phys Lett.* **1998**;287(3–4):435–441. doi: [10.1016/S0009-2614\(97\)01464-4](https://doi.org/10.1016/S0009-2614(97)01464-4)

Heliconical nematic and smectic phases: the synthesis and characterisation of the CB4O.*m* and CB8O.*m* series

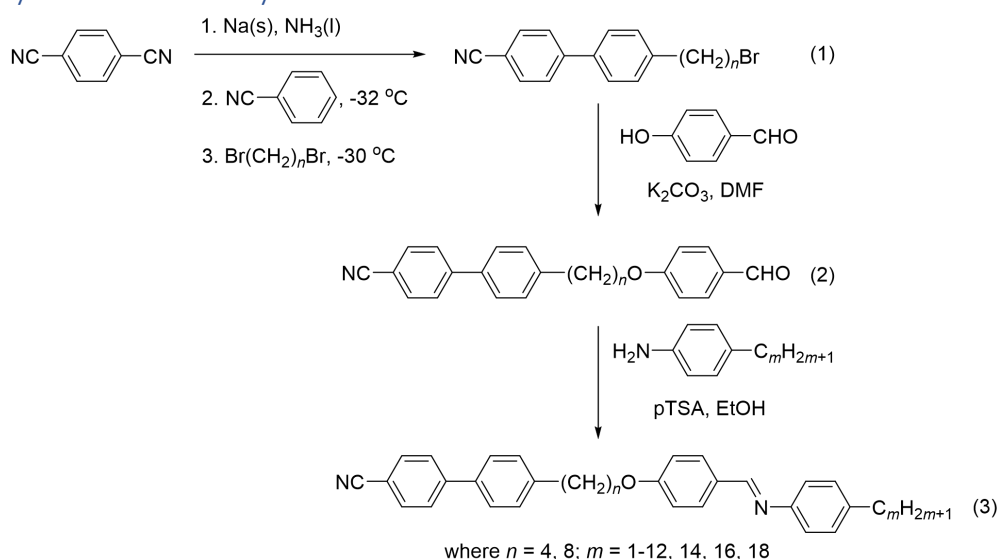
Ahlam Alshammari¹, Amerigo Zattarin¹, Abigail Pearson¹, Ewan Cruickshank¹, Magdalena Majewska², Damian Pociecha², John MD Storey¹, Ewa Gorecka², Corrie T Imrie¹ and Rebecca Walker^{1*}

¹ Department of Chemistry, School of Natural and Computing Sciences, University of Aberdeen, AB24 3UE, Aberdeen, UK

² Faculty of Chemistry, University of Warsaw, ul. Zwirki i Wigury 101, 02-089, Warsaw, Poland

Supplemental Information

1. Synthesis and Analytical Data



4'-(ω-Bromoalkyl)-[1,1'-biphenyl]-4-carbonitriles (CBnBr) (1)

Under an inert argon atmosphere, sodium (Table S1) was added to a stirred suspension of 1,4-dinitrobenzene (Table S1) in NH₃ (l) (50 ml) at -33 °C and the solution turned brown. After 5 min, benzonitrile (Table S1) was added dropwise and the reaction mixture left to stir for 30 min. 1,ω-Dibromoalkane (Table S1) was added dropwise and left to stir for 1.5 h, maintaining the acetonitrile-dry ice bath temperature at ca. -30 °C. Diethyl ether (30 ml) was added slowly, maintaining the cooling bath temperature under ca. -30 °C, and after 10 min the flask was left open to allow the NH₃ to evaporate. The reaction mixture was added to a mixture of Et₂O (30 ml) and distilled water (30 ml). The layers were separated, and the aqueous layer was washed with Et₂O (60 ml). The organic layers were combined, washed with distilled water (3 x 50 ml), and dried over anhydrous MgSO₄. The solvent was removed under vacuum, and the yellow liquid was purified by Biotage column chromatography (Et₂O:Hex [10:40]). Yields in the range of 10-19 % were obtained.

Table S1. Quantities of reagents used in the synthesis of the 4'-(ω -bromoalkyl)-[1,1'-biphenyl]-4-carbonitriles (CBnBr).

<i>n</i>	Quantity of 1,4-dinitrile benzene		Quantity of sodium metal		Quantity of benzonitrile			1, ω -dibromoalkane used	Quantity of 1, ω -dibromoalkane		
	g	mmol	g	mmol	g	mmol	mL		g	mmol	mL
4	9.6	75	3.5	155.0	11.5	112	11.5	1,4-dibromobutane	5.97	90	10.8
8	3.84	30	1.42	62.0	4.64	45	4.6	1,8-dibromooctane	9.78	36	6.7

CB4Br: MP 81 °C. ^1H NMR (400 MHz, CDCl_3) δ ppm: 7.62 (m, 4H, Ar), 7.48 (d, J = 8.0 Hz, 2H, Ar), 7.22 (d, J = 7.8 Hz, 2H, Ar), 3.37 (t, J = 6.6 Hz, 2H, $\text{ArCH}_2(\text{CH}_2)_2\text{CH}_2\text{Br}$), 2.64 (t, J = 7.8 Hz, 2H, $\text{ArCH}_2(\text{CH}_2)_2\text{CH}_2\text{Br}$), 1.82-1.79 (m, 4H, $\text{ArCH}_2(\text{CH}_2)_2\text{CH}_2\text{Br}$). ^{13}C NMR (101 MHz, CDCl_3) δ ppm: 145.49, 142.60, 136.84, 132.59, 129.17, 127.51, 127.23, 119.01, 110.66, 34.65, 33.53, 32.20, 29.73. IR $\bar{\nu}$ cm^{-1} : 2928, 2861 (aromatic CH), 2225 ($\text{C}\equiv\text{N}$).

CB8Br: MP 61 °C. ^1H NMR (400 MHz, CDCl_3) δ ppm: 7.77 – 7.66 (m, 4H, Ar), 7.54 (d, J = 8.2 Hz, 2H, Ar), 7.31 (d, J = 8.2 Hz, 2H, Ar), 3.43 (t, J = 6.8 Hz, 2H, $\text{ArCH}_2\text{CH}_2\text{CH}_2\text{CH}_2\text{CH}_2\text{CH}_2\text{CH}_2\text{CH}_2\text{Br}$), 2.69 (t, J = 8.2 Hz, 2H, $\text{ArCH}_2\text{CH}_2\text{CH}_2\text{CH}_2\text{CH}_2\text{CH}_2\text{CH}_2\text{CH}_2\text{CH}_2\text{Br}$), 1.88 (p, J = 6.9 Hz, 2H $\text{Ar}(\text{CH}_2)_6\text{CH}_2\text{CH}_2\text{Br}$), 1.68 (p, J = 7.5 Hz, 2H, $\text{ArCH}_2\text{CH}_2\text{CH}_2\text{CH}_2\text{CH}_2\text{CH}_2\text{CH}_2\text{CH}_2\text{CH}_2\text{Br}$), 1.53 – 1.29 (m, 8H, $\text{ArCH}_2\text{CH}_2\text{CH}_2\text{CH}_2\text{CH}_2\text{CH}_2\text{CH}_2\text{CH}_2\text{CH}_2\text{Br}$). ^{13}C NMR (101 MHz, CDCl_3) δ ppm: 145.63, 143.68, 136.51, 132.58, 129.19, 127.50, 127.10, 119.06, 110.56, 35.61, 34.02, 32.79, 31.33, 29.28, 29.17, 28.68, 28.14. IR $\bar{\nu}$ cm^{-1} : 2924, 2853(sp^2 C-H), 2227 (CN), 1605 (Ar-C=C aromatic), 1495 (C-H sp^2), 560 (C-Br)

4'-(ω -(4-Formylphenoxy)alkyl)-[1,1'-biphenyl]-4-carbonitriles (CBnOAH) (2)

Under an inert argon atmosphere, a mixture of 4'-(ω -bromoalkyl)-[1,1'-biphenyl]-4-carbonitrile (Table S2), 4-hydroxybenzaldehyde (Table S2), and potassium carbonate (Table S2) in dry DMF (10 mL) was heated to 90 °C for 24 h. The reaction mixture was added to water (30 mL). The precipitate was collected by vacuum filtration and washed with DCM (15 mL) and water (15 mL). The layers were separated, and the organic layer was washed with water (3 x 10 mL). The organic layers were combined and dried over anhydrous MgSO_4 , and the solvent was removed *in vacuo*, the product was recrystallised from ethanol. Yields in the range 52-65 % were obtained.

Table S2. Quantities of reagents used in the synthesis of the 4'-(ω -(4-formylphenoxy)yl)-[1,1'-biphenyl]-4-carbonitriles (CBnOAH).

<i>n</i>	Quantity of 4'-(ω -bromoalkyl)-[1,1'-biphenyl]-4-carbonitrile		Quantity of 4-hydroxybenzaldehyde		Quantity of potassium carbonate	
	g	mmol	g	mmol	g	mmol
4	2.00	6.4	0.78	6.4	1.75	12.6
8	0.79	2.1	0.29	2.3	0.59	4.2

CB4OAH: MP 124 °C. ^1H NMR (400 MHz, CDCl_3) δ ppm: 9.81 (s, 1H, ArCHO), 7.76 (d, J = 8.3 Hz, 2H, Ar), 7.62 (m, 4H, Ar), 7.45 (d, J = 7.7 Hz, 2H, Ar), 7.23 (d, J = 8.0 Hz, 2H, Ar), 6.91 (d, J = 8.3 Hz, 2H, Ar), 4.08 (t, J = 6.5 Hz, 2H, $\text{ArCH}_2\text{CH}_2\text{CH}_2\text{CH}_2\text{OAr}$), 2.70 (t, J = 7.7 Hz, 2H, $\text{ArCH}_2\text{CH}_2\text{CH}_2\text{CH}_2\text{OAr}$), 1.82-1.79 (m, 4H, $\text{ArCH}_2\text{CH}_2\text{CH}_2\text{CH}_2\text{OAr}$). ^{13}C NMR (101 MHz, CDCl_3) δ ppm: 190.77, 164.09, 145.47, 142.79,

136.82, 132.59, 132.00, 129.88, 129.20, 127.50, 127.22, 119.00, 114.72, 110.67, 68.09, 35.20, 28.66, 27.67. IR $\bar{\nu}$ cm⁻¹: 2922, 2858 (aromatic CH), 2225 (C≡N), 1675 (C=O).

CB8OAH: MP = 65 °C. ¹H NMR (400 MHz, CDCl₃) δ ppm: 9.89 (s, 1H, ArCHO), 7.84 (d, J = 8.3 Hz, 2H, Ar), 7.70 (t, J = 6.3 Hz, 4H, Ar), 7.53 (d, J = 7.8 Hz, 2H, Ar), 7.31 (d, J = 7.8 Hz, 2H, Ar), 7.00 (d, J = 8.4 Hz, 2H, Ar), 4.05 (t, J = 6.6 Hz, 2H, ArCH₂CH₂(CH₂)₄CH₂CH₂OAr), 2.69 (t, J = 7.8 Hz, 2H, ArCH₂CH₂(CH₂)₄CH₂CH₂OAr), 1.83 (p, J = 6.9 Hz, 2H, , ArCH₂CH₂(CH₂)₄CH₂CH₂OAr), 1.69 (p, J = 7.2 Hz, 2H, ArCH₂CH₂(CH₂)₄CH₂CH₂-OAr), 1.61 – 1.35 (m, 8H, ArCH₂CH₂(CH₂)₄CH₂CH₂OAr). ¹³C NMR (101 MHz, CDCl₃) δ ppm: 190.76, 164.24, 145.55, 143.70, 136.43, 132.56, 131.99, 129.78, 129.20, 127.46, 127.09, 119.05, 114.77, 110.53, 68.40, 35.63, 31.37, 29.42, 29.28, 29.25, 29.06, 25.98. IR $\bar{\nu}$ cm⁻¹: 2929, 2854, 2222 (C≡N stretch), 1681 (C=O aldehyde), 1598 (para di-substituted benzene), 1575, 1251, 1164, 1017, 816, 519.

4'-(ω -{4-[[[4-Alkylphenyl]imino]methyl]phenoxy}alkyl)[1,1'- biphenyl]-4-carbonitriles, CBnO.m (3)

Under an inert argon atmosphere, 4'-[*n*-(4-formylphenoxy)alkyl][1,1'-biphenyl]-4- carbonitrile (Table 3), the appropriate alkylaniline (Table 3) and a crystal of p-toluenesulfonic acid were combined in EtOH (10 mL) and heated at reflux for 4-5 h. The mixture was cooled to room temperature and the resulting precipitate collected by vacuum filtration. The crude product was recrystallised twice from ethanol. Yields in the range 49-86 % were obtained.

Table S3. Quantities of reagents used in the synthesis of the 4'-(ω -{4-[[[4-Alkylphenyl]imino]methyl]phenoxy}alkyl)[1,1'- biphenyl]-4-carbonitriles (CBnO.m).

<i>n</i>	<i>m</i>	Quantity of CBnOAH		Quantity of alkylaniline		
		g	mmol	g	mL	mmol
4	1	0.100	0.28	0.036	-	0.33
	2	0.100	0.28	0.040	0.041	0.33
	3	0.100	0.28	0.045	0.049	0.33
	4	0.100	0.28	0.050	0.053	0.33
	5	0.100	0.28	0.055	0.060	0.33
	6	0.100	0.28	0.060	0.065	0.33
	7	0.100	0.28	0.065	0.071	0.33
	8	0.100	0.28	0.070	0.078	0.33
	9	0.100	0.28	0.075	0.082	0.33
	10	0.100	0.28	0.080	0.085	0.33
	12	0.070	0.20	0.063	-	0.24
	14	0.070	0.20	0.069	-	0.24
	16	0.100	0.20	0.105	-	0.33
	18	0.070	0.20	0.083	-	0.24
8	1	0.191	0.46	0.060	-	0.51
	2	0.150	0.36	0.050	0.051	0.40
	3	0.150	0.36	0.054	0.059	0.40
	4	0.150	0.36	0.060	0.063	0.40
	5	0.253	0.61	0.120	0.131	0.67
	6	0.150	0.36	0.071	0.077	0.40
	7	0.150	0.51	0.077	0.085	0.40
	8	0.211	0.36	0.128	0.143	0.51
	9	0.150	0.36	0.089	0.097	0.40
	10	0.150	0.36	0.093	0.099	0.40

11	0.102	0.24	0.070	-	0.27
12	0.150	0.36	0.105	-	0.40
14	0.150	0.36	0.116	-	0.40
16	0.150	0.36	0.127	-	0.40
18	0.150	0.36	0.140	-	0.40

CB4O.1: ^1H NMR (400 MHz, CDCl_3) δ ppm: 8.42 (s, 1H, $\text{CH}=\text{N}$), 7.81 (d, $J = 8.4$ Hz, 2H, Ar), 7.71 (m, 4H, Ar), 7.55 (d, $J = 7.9$ Hz, 2H, Ar), 7.35 (d, $J = 8.0$ Hz, 2H, Ar), 7.21 (d, $J = 8.3$ Hz, 2H, Ar) 7.18 (d, $J = 8.0$ Hz, 2H, Ar), 6.99 (d, $J = 7.8$ Hz, 2H), 4.08 (t, $J = 6.5$ Hz, 2H, $\text{ArCH}_2\text{CH}_2\text{CH}_2\text{CH}_2\text{OAr}$), 2.78 (t, $J = 7.8$ Hz, 2H, $\text{ArCH}_2\text{CH}_2\text{CH}_2\text{CH}_2\text{OAr}$), 2.40 (s, 3H, ArCH_3), 1.92-1.88 (m, 4H, $\text{ArCH}_2\text{CH}_2\text{CH}_2\text{CH}_2\text{OAr}$). ^{13}C NMR (101 MHz, CDCl_3) δ ppm: 161.62, 158.95, 149.90, 145.54, 142.93, 140.54, 136.81, 132.60, 130.39, 129.74, 129.23, 127.52, 127.21, 120.77, 119.02, 114.65, 110.67, 67.84, 35.24, 28.77, 27.72, 21.00. IR $\bar{\nu}$ cm^{-1} : 2943, 2858 (aromatic CH), 2223 ($\text{C}\equiv\text{N}$), 1621 ($\text{C}=\text{N}$). Elemental Analysis for $\text{C}_{31}\text{H}_{28}\text{N}_2\text{O}$ Calculated: C = 83.75 % H = 6.35 % N = 6.30 %; Found C = 83.49 % H = 6.39 % N = 6.21 %.

CB4O.2: ^1H NMR (400 MHz, CDCl_3) δ ppm: 8.42 (s, 1H, $\text{CH}=\text{N}$), 7.81 (d, $J = 8.4$ Hz, 2H, Ar), 7.71 (m, 4H, Ar), 7.55 (d, $J = 7.9$ Hz, 2H, Ar), 7.35 (d, $J = 8.0$ Hz, 2H, Ar), 7.21 (d, $J = 8.3$ Hz, 2H, Ar) 7.18 (d, $J = 8.0$ Hz, 2H, Ar), 6.99 (d, $J = 7.8$ Hz, 2H), 4.08 (t, $J = 6.5$ Hz, 2H, $\text{ArCH}_2\text{CH}_2\text{CH}_2\text{CH}_2\text{OAr}$), 2.78 (t, $J = 7.8$ Hz, 2H, $\text{ArCH}_2\text{CH}_2\text{CH}_2\text{CH}_2\text{OAr}$), 2.63 (q, $J = 6.7$ Hz, 2H, $\text{ArCH}_2\text{CH}_2\text{CH}_3$), 1.92-1.88 (m, 4H, $\text{ArCH}_2\text{CH}_2\text{CH}_2\text{CH}_2\text{OAr}$) 1.29 (t, $J = 6.7$ Hz, 3H, $\text{ArCH}_2\text{CH}_2\text{CH}_3$). ^{13}C NMR (101 MHz, CDCl_3) δ ppm: 161.58, 158.96, 149.97, 145.54, 142.95, 141.80, 136.78, 132.60, 130.39, 129.36, 129.23, 128.54, 127.52, 127.22, 120.84, 119.03, 114.64, 110.64, 67.85, 35.24, 28.77, 28.42, 27.72, 15.68. IR $\bar{\nu}$ cm^{-1} : 2945, 2857 (aromatic CH), 2224 ($\text{C}\equiv\text{N}$), 1622 ($\text{C}=\text{N}$). Elemental Analysis for $\text{C}_{32}\text{H}_{30}\text{N}_2\text{O}$ Calculated: C = 83.81 % H = 6.59 % N = 6.11 %; Found C = 83.66 % H = 6.48 % N = 5.95 %.

CB4O.3: ^1H NMR (400 MHz, CDCl_3) δ ppm: 8.42 (s, 1H, $\text{CH}=\text{N}$), 7.81 (d, $J = 8.4$ Hz, 2H, Ar), 7.71 (m, 4H, Ar), 7.55 (d, $J = 7.9$ Hz, 2H, Ar), 7.35 (d, $J = 8.0$ Hz, 2H, Ar), 7.21 (d, $J = 8.3$ Hz, 2H, Ar) 7.18 (d, $J = 8.0$ Hz, 2H, Ar), 6.99 (d, $J = 7.8$ Hz, 2H), 4.08 (t, $J = 6.5$ Hz, 2H, $\text{ArCH}_2\text{CH}_2\text{CH}_2\text{CH}_2\text{OAr}$), 2.78 (t, $J = 7.8$ Hz, 2H, $\text{ArCH}_2\text{CH}_2\text{CH}_2\text{CH}_2\text{OAr}$), 2.63 (m, 2H, $\text{ArCH}_2\text{CH}_2\text{CH}_3$), 1.92-1.88 (m, 4H, $\text{ArCH}_2\text{CH}_2\text{CH}_2\text{CH}_2\text{OAr}$), 1.67 (m, 2H, $\text{ArCH}_2\text{CH}_2\text{CH}_3$), 0.91 (t, $J = 6.7$ Hz, 3H, $\text{ArCH}_2\text{CH}_2\text{CH}_3$). ^{13}C NMR (101 MHz, CDCl_3) δ ppm: 161.57, 158.91, 149.91, 145.54, 142.95, 140.48, 136.78, 132.60, 130.38, 129.38, 129.23, 129.09, 127.52, 127.21, 120.76, 119.03, 114.64, 110.64, 67.84, 35.22, 33.73, 28.77, 27.72, 22.37, 13.98. IR $\bar{\nu}$ cm^{-1} : 2944, 2856 (aromatic CH), 2224 ($\text{C}\equiv\text{N}$), 1605 ($\text{C}=\text{N}$). Elemental Analysis for $\text{C}_{33}\text{H}_{32}\text{N}_2\text{O}$ Calculated: C = 83.86 % H = 6.82 % N = 5.93 %; Found: C = 83.45 % H = 6.86 % N = 5.86 %.

CB4O.4: ^1H NMR (400 MHz, CDCl_3) δ ppm: 8.42 (s, 1H, $\text{CH}=\text{N}$), 7.81 (d, $J = 8.4$ Hz, 2H, Ar), 7.71 (m, 4H, Ar), 7.55 (d, $J = 7.9$ Hz, 2H, Ar), 7.35 (d, $J = 8.0$ Hz, 2H, Ar), 7.21 (d, $J = 8.3$ Hz, 2H, Ar) 7.18 (d, $J = 8.0$ Hz, 2H, Ar), 6.99 (d, $J = 7.8$ Hz, 2H), 4.08 (t, $J = 6.5$ Hz, 2H, $\text{ArCH}_2\text{CH}_2\text{CH}_2\text{CH}_2\text{OAr}$), 2.78 (t, $J = 7.8$ Hz, 2H, $\text{ArCH}_2\text{CH}_2\text{CH}_2\text{CH}_2\text{OAr}$), 2.63 (m, 2H, $\text{ArCH}_2(\text{CH}_2)_2\text{CH}_3$), 1.92-1.88 (m, 4H, $\text{ArCH}_2\text{CH}_2\text{CH}_2\text{CH}_2\text{OAr}$), 1.67 (m, 2H, $\text{ArCH}_2\text{CH}_2\text{CH}_3$), 1.36-1.32 (m, 2H, $\text{ArCH}_2\text{CH}_2\text{CH}_2\text{CH}_3$), 0.91 (t, $J = 6.7$ Hz, 3H, $\text{ArCH}_2\text{CH}_2\text{CH}_3$). ^{13}C NMR (101 MHz, CDCl_3) δ ppm: 161.57, 158.91, 149.91, 145.54, 142.95, 140.48, 136.78, 132.60, 130.38, 129.38, 129.23, 129.09, 127.52, 127.22, 120.76, 119.03, 114.64, 110.64, 67.84, 35.24, 35.19, 33.73, 28.77, 27.72, 22.37, 13.99. IR $\bar{\nu}$ cm^{-1} : 2948, 2855 (aromatic CH), 2224 ($\text{C}\equiv\text{N}$), 1605 ($\text{C}=\text{O}$). Elemental Analysis for $\text{C}_{34}\text{H}_{34}\text{N}_2\text{O}$ Calculated: C = 83.91 % H = 7.04 % N = 5.76 %; Found: C = 83.55 % H = 7.16 % N = 5.66 %.

CB4O.5: ^1H NMR (400 MHz, CDCl_3) δ ppm: 8.42 (s, 1H, $\text{CH}=\text{N}$), 7.81 (d, $J = 8.4$ Hz, 2H, Ar), 7.71 (m, 4H, Ar), 7.55 (d, $J = 7.9$ Hz, 2H, Ar), 7.35 (d, $J = 8.0$ Hz, 2H, Ar), 7.21 (d, $J = 8.3$ Hz, 2H, Ar) 7.18 (d, $J = 8.0$ Hz, 2H, Ar), 6.99 (d, $J = 7.8$ Hz, 2H), 4.08 (t, $J = 6.5$ Hz, 2H, $\text{ArCH}_2\text{CH}_2\text{CH}_2\text{CH}_2\text{OAr}$), 2.78 (t, $J = 7.8$ Hz, 2H,

ArCH₂CH₂CH₂CH₂OAr), 2.63 (t, J = 7.8 Hz, 2H, ArCH₂CH₂(CH₂)₂CH₃), 1.92-1.88 (m, 4H, ArCH₂CH₂CH₂CH₂OAr), 1.68-1.66 (m, 2H, ArCH₂CH₂(CH₂)₂CH₃), 1.36-1.32 (m, 4H, ArCH₂CH₂(CH₂)₂CH₃), 0.91 (t, J = 6.7 Hz, 3H, ArCH₂CH₂(CH₂)₂CH₃). ¹³C NMR (101 MHz, CDCl₃) δ ppm: 161.57, 158.92, 149.91, 145.54, 142.95, 140.52, 136.78, 132.60, 130.38, 129.37, 129.23, 129.08, 127.52, 127.22, 120.76, 119.03, 114.64, 110.64, 67.84, 35.47, 35.24, 31.52, 31.26, 28.77, 27.73, 22.57, 14.06. IR $\bar{\nu}$ cm⁻¹: 2944, 2830 (aromatic CH), 2224 (C≡N), 1622 (C=N). Elemental Analysis for C₃₅H₃₆N₂O Calculated: C = 83.94 % H = 7.25 % N = 5.60 %; Found C = 83.65 % H = 7.41 % N = 5.59 %.

CB40.6: ¹H NMR (400 MHz, CDCl₃) δ ppm: 8.39 (s, 1H, CH=N), 7.83 (d, J = 8.6 Hz, 2H, Ar), 7.69 (m, 4H, Ar), 7.52 (d, J = 8.0 Hz, 2H, Ar), 7.32 (d, J = 8.1 Hz, 2H, Ar), 7.19 (d, J = 8.2 Hz, 2H, Ar), 7.13 (d, J = 8.4 Hz, 2H, Ar), 6.96 (d, J = 8.5 Hz, 2H, Ar), 4.06 (t, J = 6.5 Hz, 2H, ArCH₂CH₂CH₂CH₂OAr), 2.76 (t, J = 7.8 Hz, 2H, ArCH₂CH₂CH₂CH₂OAr), 2.62 (t, J = 7.7 Hz, 2H, ArCH₂CH₂(CH₂)₃CH₃), 1.90-1.86 (m, 4H, ArCH₂CH₂CH₂CH₂OAr), 1.68-1.58 (m, 2H, ArCH₂CH₂(CH₂)₃CH₃), 1.39 – 1.26 (m, 6H, ArCH₂CH₂(CH₂)₃CH₃), 0.93-0.82 (m, 3H, ArCH₂CH₂(CH₂)₃CH₃). ¹³C NMR (101 MHz, CDCl₃) δ ppm: 161.58, 158.92, 145.54, 142.95, 140.55, 136.78, 132.60, 130.40, 129.36, 129.23, 129.09, 127.52, 127.22, 120.76, 119.04, 114.65, 110.64, 67.85, 35.51, 35.24, 31.76, 31.55, 29.00, 28.77, 27.72, 22.64, 14.12. IR $\bar{\nu}$ cm⁻¹: 2944, 2840 (aromatic CH), 2224 (C≡N), 1622 (C=N). Elemental Analysis for C₃₆H₃₈N₂O Calculated: C = 84.01 % H = 7.44 % N = 5.44 %; Found: C = 83.55 % H = 7.51 % N = 5.13 %.

CB40.7: ¹H NMR (400 MHz, CDCl₃) δ ppm: 8.42 (s, 1H, CH=N), 7.81 (d, J = 8.4 Hz, 2H, Ar), 7.71 (m, 4H, Ar), 7.55 (d, J = 7.9 Hz, 2H, Ar), 7.35 (d, J = 8.0 Hz, 2H, Ar), 7.21 (d, J = 8.3 Hz, 2H, Ar) 7.18 (d, J = 8.0 Hz, 2H, Ar), 6.99 (d, J = 7.8 Hz, 2H), 4.08 (t, J = 6.5 Hz, 2H, ArCH₂CH₂CH₂CH₂OAr), 2.78 (t, J = 7.8 Hz, 2H, ArCH₂CH₂CH₂CH₂OAr), 2.68 (t, J = 7.8 Hz, 2H, ArCH₂CH₂(CH₂)₄CH₃), 1.92-1.88 (m, 4H, ArCH₂CH₂CH₂CH₂OAr), 1.68-1.66 (m, 2H, ArCH₂CH₂(CH₂)₄CH₃), 1.36-1.33 (m, 8H, ArCH₂CH₂(CH₂)₄CH₃), 0.92 (t, J = 6.7 Hz, 3H, ArCH₂CH₂(CH₂)₄CH₃). ¹³C NMR (101 MHz, CDCl₃) δ ppm: 161.57, 158.91, 149.90, 145.54, 142.95, 140.54, 136.78, 132.60, 130.39, 129.37, 129.23, 129.08, 127.52, 127.22, 120.76, 119.03, 114.64, 110.64, 67.85, 35.51, 35.24, 31.85, 31.59, 29.29, 29.21, 28.78, 27.73, 22.68, 14.12. IR $\bar{\nu}$ cm⁻¹: 2944, 2856 (aromatic CH), 2224 (C≡N), 1623 (C=N). Elemental Analysis for C₃₇H₄₀N₂O Calculated: C = 84.05 % H = 7.63 % N = 5.30 %; Found: C = 83.55 % H = 7.51 % N = 5.13 %.

CB40.8: ¹H NMR (400 MHz, CDCl₃) δ ppm: 8.42 (s, 1H, CH=N), 7.81 (d, J = 8.4 Hz, 2H, Ar), 7.71 (m, 4H, Ar), 7.55 (d, J = 7.9 Hz, 2H, Ar), 7.35 (d, J = 8.0 Hz, 2H, Ar), 7.21 (d, J = 8.3 Hz, 2H, Ar) 7.18 (d, J = 8.0 Hz, 2H, Ar), 6.99 (d, J = 7.8 Hz, 2H), 4.08 (t, J = 6.5 Hz, 2H, ArCH₂CH₂CH₂CH₂OAr), 2.78 (t, J = 7.8 Hz, 2H, ArCH₂CH₂CH₂CH₂OAr), 2.63 (m, 2H, ArCH₂CH₂(CH₂)₅CH₃), 1.92-1.88 (m, 4H, ArCH₂CH₂CH₂CH₂OAr), 1.68-1.66 (m, 2H, ArCH₂CH₂(CH₂)₅CH₃), 1.36-1.33 (m, 10H, ArCH₂CH₂(CH₂)₅CH₃), 0.92 (t, J = 6.7 Hz, 3H, ArCH₂CH₂(CH₂)₅CH₃). ¹³C NMR (101 MHz, CDCl₃) δ ppm: 161.58, 158.96, 149.97, 145.54, 142.95, 141.80, 136.77, 132.60, 130.39, 129.36, 129.29, 128.54, 127.52, 127.21, 120.83, 119.03, 114.64, 110.64, 67.84, 35.24, 28.77, 28.42, 27.72, 15.68. IR $\bar{\nu}$ cm⁻¹: 2926, 2854 (aromatic CH), 2225 (C≡N), 1623 (C=N). Elemental Analysis for C₃₈H₄₂N₂O Calculated: C = 84.09 % H = 7.80 % N = 5.16 %; Found: C = 83.75 % H = 7.92 % N = 5.14 %.

CB40.9: ¹H NMR (400 MHz, CDCl₃) δ ppm: 8.32 (s, 1H, CH=N), 7.75 (d, J = 8.4 Hz, 2H, Ar), 7.62 (m, 4H, Ar), 7.45 (d, J = 8.0 Hz, 2H, Ar), 7.25 (d, J = 7.9 Hz, 2H, Ar), 7.12 (d, J = 8.1 Hz, 2H, Ar), 7.05 (d, J = 8.0 Hz, 2H, Ar), 6.89 (d, J = 8.2 Hz, 2H, Ar), 3.99 (t, J = 7.8 Hz, 2H, ArCH₂CH₂CH₂CH₂OAr), 2.70 (t, J = 7.8 Hz, 2H, ArCH₂CH₂CH₂CH₂OAr), 2.54 (t, J = 7.7 Hz, 2H, ArCH₂CH₂(CH₂)₆CH₃), 1.82-1.80 (m, 4H, ArCH₂CH₂CH₂CH₂OAr), 1.57-1.54 (m, 2H, ArCH₂CH₂(CH₂)₆CH₃), 1.26-1.22 (m, 12H, ArCH₂CH₂(CH₂)₆CH₃), 0.81 (t, J = 6.7 Hz, 3H, ArCH₂CH₂(CH₂)₆CH₃). ¹³C NMR (101 MHz, CDCl₃) δ ppm: 161.57, 158.91, 149.90, 145.54, 142.95, 140.54, 136.78, 132.60, 130.38, 129.38, 129.23, 129.08, 127.52, 127.22, 120.76, 119.03, 114.64, 110.64, 67.84, 35.51, 35.24, 31.92, 31.59, 29.58, 29.55, 29.35, 29.33, 28.78, 27.73,

22.70, 14.13. IR $\bar{\nu}$ cm⁻¹: 2944 (aromatic CH), 2224 (C≡N), 1622 (C=N). Elemental Analysis for C₃₉H₄₄N₂O Calculated: C = 84.13 % H = 7.97 % N = 5.03 %; Found: C = 83.65 % H = 8.05 % N = 5.00 %.

CB40.10: ¹H NMR (400 MHz, CDCl₃) δ ppm: 8.39 (s, 1H, CH=N), 7.82 (d, *J* = 8.3 Hz, 2H, Ar), 7.70 (m, 4H, Ar), 7.53 (d, *J* = 7.6 Hz, 2H, Ar), 7.33 (d, *J* = 7.8 Hz, 2H, Ar), 7.17 (d, *J* = 7.9 Hz, 2H), 7.11 (d, *J* = 7.9 Hz, 2H), 6.97 (d, *J* = 8.1 Hz, 2H, Ar), 4.05 (t, *J* = 5.9 Hz, 2H, ArCH₂CH₂CH₂CH₂OAr), 2.77 (t, *J* = 6.0 Hz, 2H, ArCH₂CH₂CH₂CH₂OAr), 2.61 (t, *J* = 8.0 Hz, 2H, ArCH₂CH₂(CH₂)₇CH₃), 1.91 – 1.85 (m, 4H, ArCH₂CH₂CH₂CH₂OAr), 1.62 (m, 2H, ArCH₂CH₂(CH₂)₇CH₃), 1.33–1.28 (m, 14H, ArCH₂CH₂(CH₂)₇CH₃), 0.88 (t, *J* = 6.4 Hz, 3H, ArCH₂CH₂(CH₂)₇CH₃). ¹³C NMR (101 MHz, CDCl₃) δ ppm: 161.53, 158.91, 149.81, 145.54, 142.95, 140.50, 136.78, 132.60, 130.38, 129.40, 129.23, 129.08, 127.52, 127.21, 120.76, 119.03, 114.64, 110.64, 67.85, 35.51, 35.24, 31.92, 31.58, 29.64, 29.62, 29.54, 29.36, 29.33, 28.77, 27.73, 22.70, 14.14. IR $\bar{\nu}$ cm⁻¹: 2944 (aromatic CH), 2224 (C≡N), 1622 (C=N). Elemental Analysis for C₄₀H₄₆N₂O Calculated: C = 84.17 % H = 8.12 % N = 4.91 %; Found: C = 83.80 % H = 8.05 % N = 4.73 %.

CB40.12: ¹H NMR (400 MHz, CDCl₃) δ ppm: 8.40 (s, 1H, CH=N), 7.83 (d, *J* = 8.4 Hz, 2H, Ar), 7.69 (m, 4H, Ar), 7.53 (d, *J* = 7.9 Hz, 2H, Ar), 7.32 (d, *J* = 7.9 Hz, 2H, Ar), 7.20 – 7.10 (m, 4H, Ar), 6.96 (d, *J* = 8.5 Hz, 2H, Ar), 4.06 (m, 2H, ArCH₂CH₂CH₂CH₂OAr), 2.81 – 2.73 (m, 2H, ArCH₂CH₂CH₂CH₂OAr), 2.62 (t, *J* = 7.7 Hz, 2H, ArCH₂CH₂(CH₂)₉CH₃), 1.88 (m, 4H, ArCH₂CH₂CH₂CH₂OAr), 1.62 (m, 2H, ArCH₂CH₂(CH₂)₉CH₃), 1.33 (m, 18H, ArCH₂CH₂(CH₂)₉CH₃), 0.89 (t, *J* = 6.6 Hz, 3H, ArCH₂CH₂(CH₂)₉CH₃). ¹³C NMR (101 MHz, CDCl₃) δ ppm: 161.57, 158.90, 149.90, 145.54, 142.95, 140.54, 136.77, 132.60, 130.39, 129.38, 129.23, 129.09, 127.52, 127.22, 120.77, 119.04, 114.65, 110.64, 67.85, 35.52, 35.25, 31.95, 31.59, 29.71, 29.69, 29.67, 29.63, 29.55, 29.38, 29.34, 28.78, 27.73, 22.72, 14.15. IR $\bar{\nu}$ cm⁻¹: 2932 (aromatic CH), 2227 (C≡N), 1621 (C=N). HRMS: (TOF ESI+) (*m/z*): [M+H]⁺ for C₄₂H₅₁N₂O Calculated: 599.4001; Found: 599.3993 (1.3 ppm difference).

CB40.14: ¹H NMR (400 MHz, CDCl₃) δ ppm: 8.39 (s, 1H, CH=N), 7.86 – 7.77 (m, 2H, Ar), 7.69 (m, 4H, Ar), 7.59 – 7.49 (m, 2H, Ar), 7.36 – 7.29 (m, 2H, Ar), 7.22 – 7.10 (m, 4H, Ar), 6.97 (m, 2H, Ar), 4.06 (m, 2H, ArCH₂CH₂CH₂CH₂OAr), 2.77 (m, 2H, ArCH₂CH₂CH₂CH₂OAr), 2.66 – 2.57 (m, 2H, ArCH₂CH₂(CH₂)₁₁CH₃), 1.91 – 1.81 (m, *J* = 4.3 Hz, 4H, ArCH₂CH₂CH₂CH₂OAr), 1.66 – 1.57 (m, 2H, ArCH₂CH₂(CH₂)₁₁CH₃), 1.26 (s, 22H, ArCH₂CH₂(CH₂)₁₁CH₃), 0.88 (t, *J* = 6.7 Hz, 3H, ArCH₂CH₂(CH₂)₁₁CH₃). ¹³C NMR (101 MHz, CDCl₃) δ ppm: 161.57, 158.90, 149.90, 145.54, 142.95, 140.54, 136.77, 132.60, 130.39, 129.38, 129.23, 129.08, 128.75, 127.52, 127.22, 120.76, 119.04, 114.76, 114.64, 110.64, 77.35, 77.04, 76.72, 67.84, 35.94, 35.52, 35.25, 31.95, 31.59, 29.72, 29.70, 29.69, 29.63, 29.55, 29.38, 29.34, 28.78, 27.73, 22.71, 14.15. IR $\bar{\nu}$ cm⁻¹: 2921 (aromatic CH), 2225 (C≡N), 1622 (C=N). HRMS: (TOF ESI+) (*m/z*): [M+H]⁺ for C₄₄H₅₅N₂O Calculated: 627.4314; Found: 627.4296 (2.9 ppm difference).

CB40.16: ¹H NMR (400 MHz, CDCl₃) δ ppm: 8.39 (s, 1H, CH=N), 7.82 (d, *J* = 8.7 Hz, 2H, Ar), 7.69 (q, *J* = 8.4 Hz, 4H, Ar), 7.53 (d, *J* = 8.1 Hz, 2H, Ar), 7.32 (d, *J* = 8.1 Hz, 2H, Ar), 7.19 (d, *J* = 8.3 Hz, 2H, Ar), 7.12 (d, *J* = 8.3 Hz, 2H, Ar), 6.96 (d, *J* = 8.7 Hz, 2H, Ar), 4.06 (t, *J* = 5.8 Hz, 2H, ArCH₂CH₂CH₂CH₂OAr), 2.77 (t, *J* = 7.8 Hz, 2H, ArCH₂CH₂CH₂CH₂OAr), 2.61 (t, *J* = 7.5 Hz, 2H, ArCH₂CH₂(CH₂)₁₃CH₃), 1.91–1.85 (m, 4H, ArCH₂CH₂CH₂CH₂OAr), 1.61 (m, 2H, ArCH₂CH₂(CH₂)₁₃CH₃), 1.36–1.22 (m, 26H, ArCH₂CH₂(CH₂)₁₃CH₃), 0.88 (t, *J* = 6.6 Hz, 3H, ArCH₂CH₂(CH₂)₁₃CH₃). ¹³C NMR (101 MHz, CDCl₃) δ ppm: 161.57, 158.92, 149.89, 145.55, 142.95, 140.55, 136.78, 132.60, 130.38, 129.37, 129.23, 129.08, 127.52, 127.22, 120.76, 119.03, 114.64, 110.64, 67.84, 35.51, 35.24, 31.94, 31.59, 30.95, 29.72, 29.70, 29.68, 29.63, 29.54, 29.38, 29.33, 28.78, 27.73, 22.71, 14.14. IR $\bar{\nu}$ cm⁻¹: 2920 (aromatic CH), 2228 (C≡N), 1623 (C=N). Elemental Analysis for C₄₆H₅₈N₂O Calculated: C = 84.35 % H = 8.93 % N = 4.28 % Found: C = 84.35 % H = 9.06 % N = 4.15 %.

CB40.18: ¹H NMR (400 MHz, CDCl₃) δ ppm: 8.39 (s, 1H, CH=N), 7.86 – 7.75 (m, 2H, Ar), 7.75 – 7.64 (m, 4H, Ar), 7.58 – 7.49 (m, 2H, Ar), 7.33 (m, 2H, Ar), 7.22 – 7.09 (m, 4H, Ar), 7.05 – 6.92 (m, 2H, Ar),

4.06 (t, $J = 4.9$ Hz, 2H, $\text{ArCH}_2\text{CH}_2\text{CH}_2\text{CH}_2\text{OAr}$), 2.77 (d, $J = 7.0$ Hz, 2H, $\text{ArCH}_2\text{CH}_2\text{CH}_2\text{CH}_2\text{OAr}$), 2.65 – 2.57 (m, 2H, $\text{ArCH}_2\text{CH}_2(\text{CH}_2)_{15}\text{CH}_3$), 1.88 (p, $J = 3.0$ Hz, 4H, $\text{ArCH}_2\text{CH}_2\text{CH}_2\text{CH}_2\text{OAr}$), 1.61 (m, 2H, $\text{ArCH}_2\text{CH}_2(\text{CH}_2)_{15}\text{CH}_3$), 1.25 (m, 30H, $\text{ArCH}_2\text{CH}_2(\text{CH}_2)_{15}\text{CH}_3$), 0.92 – 0.84 (m, 3H, $\text{ArCH}_2\text{CH}_2(\text{CH}_2)_{15}\text{CH}_3$). ^{13}C NMR (101 MHz, CDCl_3) δ 161.57, 160.08, 158.90, 149.90, 145.54, 143.04, 142.95, 140.77, 140.54, 136.77, 136.74, 136.12, 132.60, 131.18, 130.39, 129.38, 129.25, 129.23, 129.08, 128.75, 127.52, 127.21, 126.91, 125.73, 120.76, 119.03, 118.47, 114.76, 114.64, 110.64, 67.84, 35.94, 35.52, 35.24, 31.95, 31.59, 31.31, 29.72, 29.70, 29.68, 29.63, 29.55, 29.38, 29.34, 28.84, 28.78, 27.73, 22.71, 14.15. IR $\bar{\nu}$ cm^{-1} : 2925 (aromatic CH), 2225 ($\text{C}\equiv\text{N}$), 1622 ($\text{C}=\text{N}$). HRMS: (TOF ESI+) (m/z): $[\text{M}+\text{H}]^+$ for $\text{C}_{48}\text{H}_{63}\text{N}_2\text{O}$ Calculated: 683.4940; Found: 683.4929 (1.6 ppm difference).

CB80.1: ^1H NMR (400 MHz, CDCl_3) δ ppm: 8.41 (s, 1H, $\text{CH}=\text{N}$), 7.84 (d, $J = 8.7$ Hz, 2H, Ar), 7.71 (m, 4H, Ar), 7.53 (d, $J = 8.2$ Hz, 2H, Ar), 7.31 (d, $J = 8.1$ Hz, 2H, Ar), 7.21 (d, $J = 8.2$ Hz, 2H, Ar), 7.14 (d, $J = 8.3$ Hz, 2H, Ar), 6.98 (d, $J = 8.8$ Hz, 2H, Ar), 4.04 (t, $J = 6.5$ Hz, 2H, $\text{ArCH}_2\text{CH}_2\text{CH}_2\text{CH}_2\text{CH}_2\text{CH}_2\text{CH}_2\text{CH}_2\text{OAr}$), 2.69 (t, $J = 8.1$ Hz, 2H, $\text{ArCH}_2(\text{CH}_2)_7\text{OAr}$), 2.39 (s, 3H, ArCH_3), 1.83 (p, $J = 6.7$ Hz, 2H, $\text{Ar}(\text{CH}_2)_6\text{CH}_2\text{CH}_2\text{OAr}$), 1.71–1.65 (m, 2H, $\text{ArCH}_2\text{CH}_2(\text{CH}_2)_6\text{OAr}$), 1.54–1.19 (m, 8H, $\text{ArCH}_2\text{CH}_2\text{CH}_2\text{CH}_2\text{CH}_2\text{CH}_2\text{CH}_2\text{CH}_2\text{OAr}$). ^{13}C NMR (101 MHz, CDCl_3) δ ppm: 161.71, 158.99, 149.8, 144.6, 143.72, 136.50, 135.34, 132.58, 130.38, 129.73, 129.19, 127.49, 127.10, 120.78, 119.05, 114.66, 110.51, 68.13, 35.62, 31.36, 29.39, 29.21, 29.15, 25.99, 21.00. IR $\bar{\nu}$ cm^{-1} : 2920, 2851 ($\text{C}-\text{H}$, sp^2), 2222 ($\text{C}\equiv\text{N}$ stretch), 1622 ($\text{C}=\text{N}$), 1603 (para disubstituted benzene), 1511, 1252, 1164, 816, 537. Elemental Analysis for $\text{C}_{35}\text{H}_{36}\text{N}_2\text{O}$ Calculated: C = 83.95 %, H = 7.25 %, N = 5.60 %; Found: C = 83.68 %, H = 7.11 %, N = 5.40 %.

CB80.2: ^1H NMR (400 MHz, CDCl_3) δ ppm: 8.41 (s, 1H, $\text{CH}=\text{N}$), 7.85 (d, $J = 8.7$ Hz, 2H, Ar), 7.71 (m, 4H, Ar), 7.53 (d, $J = 8.2$ Hz, 2H, Ar), 7.31 (d, $J = 8.1$ Hz, 2H, Ar), 7.24 (d, $J = 8.3$ Hz, 2H, Ar), 7.16 (d, $J = 8.3$ Hz, 2H, Ar), 6.98 (d, $J = 8.7$ Hz, 2H, Ar), 4.04 (t, $J = 6.5$ Hz, 2H, $\text{ArCH}_2\text{CH}_2\text{CH}_2\text{CH}_2\text{CH}_2\text{CH}_2\text{CH}_2\text{CH}_2\text{OAr}$), 2.90–2.57 (m, 4H, $\text{ArCH}_2(\text{CH}_2)_7\text{OAr}$, $\text{ArCH}_2\text{CH}_2\text{CH}_3$), 1.83 (p, $J = 6.6$ Hz, 2H, $\text{Ar}(\text{CH}_2)_6\text{CH}_2\text{CH}_2\text{OAr}$), 1.79–1.61 (m, 2H, $\text{ArCH}_2\text{CH}_2(\text{CH}_2)_6\text{OAr}$), 1.55–1.31 (m, 8H, $\text{ArCH}_2\text{CH}_2\text{CH}_2\text{CH}_2\text{CH}_2\text{CH}_2\text{CH}_2\text{CH}_2\text{OAr}$), 1.28 (t, $J = 7.6$ Hz, 3H, ArCH_2CH_3). ^{13}C NMR (101 MHz, CDCl_3) δ ppm: 161.71, 159.03, 149.99, 145.62, 143.72, 141.78, 136.50, 132.58, 130.39, 129.24, 129.19, 128.53, 127.49, 127.10, 120.84, 119.06, 114.66, 110.55, 68.13, 35.62, 31.62, 29.39, 29.26, 29.21, 29.15, 28.42, 25.99, 15.68. IR $\bar{\nu}$ cm^{-1} : 2922, 2854 ($\text{C}-\text{H}$, sp^2), 2222 ($\text{C}\equiv\text{N}$ stretch), 1623 ($\text{C}=\text{N}$), 1604 (para disubstituted benzene), 1511, 1248, 1160, 818, 536. Elemental Analysis for $\text{C}_{36}\text{H}_{38}\text{N}_2\text{O}$ Calculated: C = 84.01 %, H = 7.44 %, N = 5.44 %; Found: C = 84.06 %, H = 7.41 %, N = 5.31 %.

CB80.3: ^1H NMR (400 MHz, CDCl_3) δ ppm: 8.42 (s, 1H, $\text{CH}=\text{N}$), 7.84 (d, $J = 8.7$ Hz, 2H, Ar), 7.71 (m, 4H, Ar), 7.53 (d, $J = 8.1$ Hz, 2H, Ar), 7.31 (d, $J = 8.1$ Hz, 2H, Ar), 7.21 (d, $J = 8.2$ Hz, 2H, Ar), 7.15 (d, $J = 8.3$ Hz, 2H, Ar), 6.98 (d, $J = 8.7$ Hz, 2H, Ar), 4.04 (t, $J = 6.5$ Hz, 2H, $\text{ArCH}_2\text{CH}_2\text{CH}_2\text{CH}_2\text{CH}_2\text{CH}_2\text{CH}_2\text{CH}_2\text{OAr}$), 2.73–2.58 (m, 4H, $\text{ArCH}_2(\text{CH}_2)_7\text{OAr}$, $\text{ArCH}_2\text{CH}_2\text{CH}_3$), 1.83 (p, $J = 6.7$ Hz, 2H, $\text{Ar}(\text{CH}_2)_6\text{CH}_2\text{CH}_2\text{OAr}$), 1.75–1.63 (m, 4H, $\text{ArCH}_2\text{CH}_2(\text{CH}_2)_6\text{OAr}$, $\text{ArCH}_2\text{CH}_2\text{CH}_3$), 1.45 (m, 8H, $\text{ArCH}_2\text{CH}_2\text{CH}_2\text{CH}_2\text{CH}_2\text{CH}_2\text{CH}_2\text{CH}_2\text{OAr}$), 0.98 (t, $J = 7.3$ Hz, 3H, $\text{ArCH}_2\text{CH}_2\text{CH}_3$). ^{13}C NMR (101 MHz, CDCl_3) δ ppm: 161.79, 158.98, 149.73, 145.66, 143.72, 140.22, 136.50, 134.54, 132.58, 130.37, 129.19, 129.14, 127.49, 127.10, 120.75, 118.98, 114.66, 110.54, 68.13, 37.59, 35.62, 31.36, 29.39, 29.26, 29.21, 29.15, 25.99, 24.64, 13.83. IR $\bar{\nu}$ cm^{-1} : 2923, 2853 ($\text{C}-\text{H}$, sp^2), 2223 ($\text{C}\equiv\text{N}$ stretch), 1623 ($\text{C}=\text{N}$), 1604 (para disubstituted benzene), 1510, 1249, 1160, 818, 541. Elemental Analysis for $\text{C}_{37}\text{H}_{40}\text{N}_2\text{O}$ Calculated: C = 84.05 %, H = 7.63 %, N = 5.30 %; Found: C = 84.27 %, H = 7.47 %, N = 5.17 %.

CB80.4: ^1H NMR (400 MHz, CDCl_3) δ ppm: 8.42 (s, 1H, $\text{CH}=\text{N}$), 7.84 (d, $J = 8.7$ Hz, 2H, Ar), 7.71 (m, 4H, Ar), 7.53 (d, $J = 8.2$ Hz, 2H, Ar), 7.31 (d, $J = 8.2$ Hz, 2H, Ar), 7.21 (d, $J = 8.3$ Hz, 2H, Ar), 7.15 (d, $J = 8.3$

H₂, 2H, Ar), 6.98 (d, J = 8.7 Hz, 2H, Ar), 4.04 (t, J = 6.5 Hz, 2H, ArCH₂CH₂CH₂CH₂CH₂CH₂CH₂CH₂OAr), 2.73–2.61 (m, 4H, ArCH₂(CH₂)₇OAr, ArCH₂CH₂CH₂CH₂CH₃), 1.83 (p, J = 6.6 Hz, 2H, Ar(CH₂)₆CH₂CH₂OAr), 1.72–1.56 (m, 4H, ArCH₂CH₂(CH₂)₆OAr, ArCH₂CH₂CH₂CH₂CH₃), 1.54–1.16 (m, 10H, ArCH₂CH₂CH₂CH₂CH₂CH₂CH₂CH₂CH₂OAr, ArCH₂CH₂CH₂CH₂CH₃), 0.96 (t, J = 7.3 Hz, 3H, ArCH₂CH₂CH₂CH₂CH₃). ¹³C NMR (101 MHz, CDCl₃) δ ppm: 161.70, 158.97, 149.94, 145.62, 143.72, 140.45, 136.50, 132.58, 130.38, 129.26, 129.20, 129.08, 127.49, 127.10, 120.76, 119.06, 114.66, 110.55, 68.13, 35.62, 35.19, 33.73, 31.36, 29.39, 29.26, 29.21, 29.16, 26.00, 22.37, 13.99. IR $\bar{\nu}$ cm⁻¹: 2923, 2853 (C-H, sp²), 2226 (C≡N stretch), 1624 (C=N), 1606 (para disubstituted benzene), 1511, 1259, 1164, 818, 538. Elemental Analysis for C₃₈H₄₂N₂O Calculated: C = 84.09 %, H = 7.80 %, N = 5.16 %; Found: C = 84.04 %, H = 7.70 %, N = 5.05 %.

CB80.5: ¹H NMR (400 MHz, CDCl₃) δ ppm: 8.42 (s, 1H, CH=N), 7.85 (d, J = 8.6 Hz, 2H, Ar), 7.71 (m, 4H, Ar), 7.53 (d, J = 8.2 Hz, 2H, Ar), 7.31 (d, J = 8.1 Hz, 2H, Ar), 7.21 (d, J = 8.3 Hz, 2H, Ar), 7.16 (d, J = 8.3 Hz, 2H, Ar), 6.98 (d, J = 8.7 Hz, 2H, Ar), 4.04 (t, J = 6.5 Hz, 2H, ArCH₂CH₂CH₂CH₂CH₂CH₂CH₂CH₂OAr), 2.73–2.60 (m, 4H, ArCH₂(CH₂)₇OAr, ArCH₂CH₂CH₂CH₂CH₂CH₃), 1.83 (p, J = 6.6 Hz, 2H, Ar(CH₂)₆CH₂CH₂OAr), 1.72–1.65 (m, 4H, ArCH₂CH₂(CH₂)₆OAr, ArCH₂CH₂CH₂CH₂CH₂CH₃), 1.55–1.13 (m, 12H, ArCH₂CH₂CH₂CH₂CH₂CH₂CH₂CH₂CH₂OAr, ArCH₂CH₂CH₂CH₂CH₂CH₃), 0.93 (t, J = 7.0 Hz, 3H, ArCH₂CH₂CH₂CH₂CH₃). ¹³C NMR (101 MHz, CDCl₃) δ ppm: 161.77, 158.99, 149.84, 145.62, 143.72, 140.50, 136.50, 132.58, 130.46, 129.20, 129.10, 127.49, 120.77, 119.05, 114.68, 110.54, 68.15, 35.63, 35.48, 31.52, 31.37, 31.26, 29.40, 29.27, 29.16, 26.00, 22.58, 14.07. IR $\bar{\nu}$ cm⁻¹: 2921, 2850 (C-H, sp²), 2225 (C≡N stretch), 1624 (C=N), 1606 (para disubstituted benzene), 1513, 1254, 1163, 812, 538. Elemental Analysis for C₃₉H₄₄N₂O Calculated: C = 84.13 %, H = 7.97 %, N = 5.03 %; Found: C = 83.99 %, H = 7.83 %, N = 4.94 %.

CB80.6: ¹H NMR (400 MHz, CDCl₃) δ ppm: 8.42 (s, 1H, CH=N), 7.84 (d, J = 8.7 Hz, 2H, Ar), 7.71 (m, 4H, Ar), 7.53 (d, J = 8.2 Hz, 2H, Ar), 7.31 (d, J = 8.2 Hz, 2H, Ar), 7.21 (d, J = 8.3 Hz, 2H, Ar), 7.15 (d, J = 8.3 Hz, 2H, Ar), 6.97 (d, J = 8.8 Hz, 2H, Ar), 4.04 (t, J = 6.5 Hz, 2H, ArCH₂CH₂CH₂CH₂CH₂CH₂CH₂CH₂OAr), 2.92–2.46 (m, 4H, ArCH₂(CH₂)₇OAr, ArCH₂CH₂CH₂CH₂CH₂CH₂CH₃), 1.83 (p, J = 6.2 Hz, 2H, Ar(CH₂)₆CH₂CH₂OAr), 1.72–1.59 (m, 4H, ArCH₂CH₂(CH₂)₆OAr, ArCH₂CH₂CH₂CH₂CH₂CH₃), 1.55–1.20 (m, 14H, ArCH₂CH₂CH₂CH₂CH₂CH₂CH₂CH₂CH₂OAr, ArCH₂CH₂CH₂CH₂CH₂CH₂CH₃), 0.91 (t, J = 6.7 Hz, 3H, ArCH₂CH₂CH₂CH₂CH₂CH₃). ¹³C NMR (101 MHz, CDCl₃) δ ppm: 161.70, 158.98, 149.92, 145.62, 143.72, 140.51, 136.50, 132.58, 130.38, 129.25, 129.20, 129.08, 127.49, 127.10, 120.76, 119.06, 114.66, 110.55, 68.13, 35.62, 35.51, 31.75, 31.55, 31.36, 29.26, 29.21, 29.16, 28.99, 26.00, 22.64, 14.12. IR $\bar{\nu}$ cm⁻¹: 2919, 2849 (C-H, sp²), 2226 (C≡N stretch), 1618 (C=N), 1606 (para disubstituted benzene), 1511, 1259, 1165, 815, 539. Elemental Analysis for C₄₀H₄₆N₂O Calculated: C = 84.17 %, H = 8.12 %, N = 4.91%; Found: C = 84.22 %, H = 7.96 %, N = 4.79 %.

CB80.7: ¹H NMR (400 MHz, CDCl₃) δ ppm: 8.42 (s, 1H, CH=N), 7.85 (d, J = 8.6 Hz, 2H, Ar), 7.71 (m, 4H, Ar), 7.31 (d, J = 8.2 Hz, 2H, Ar), 7.21 (d, J = 8.3 Hz, 2H, Ar), 7.15 (d, J = 8.3 Hz, 2H, Ar), 6.98 (d, J = 8.8 Hz, 2H, Ar), 4.04 (t, J = 6.5 Hz, 2H, ArCH₂CH₂CH₂CH₂CH₂CH₂CH₂CH₂OAr), 2.73–2.60 (m, 4H, ArCH₂(CH₂)₇OAr, ArCH₂CH₂CH₂CH₂CH₂CH₂CH₃), 1.82 (p, J = 6.7 Hz, 2H, Ar(CH₂)₆CH₂CH₂OAr), 1.75–1.59 (m, 4H, ArCH₂CH₂(CH₂)₆OAr, ArCH₂CH₂CH₂CH₂CH₂CH₃), 1.55–1.18 (m, 16H, ArCH₂CH₂CH₂CH₂CH₂CH₂CH₂CH₂CH₂OAr, ArCH₂CH₂CH₂CH₂CH₂CH₂CH₃), 0.91 (t, J = 6.8 Hz, 3H, ArCH₂CH₂CH₂CH₂CH₂CH₃). ¹³C NMR (101 MHz, CDCl₃) δ ppm: 161.68, 158.97, 149.97, 145.58, 143.72, 140.51, 136.45, 132.58, 130.38, 129.20, 129.08, 127.49, 127.10, 120.76, 119.07, 114.66, 110.56, 68.14, 35.62, 35.51, 31.85, 31.59, 31.36, 29.39, 29.29, 29.27, 29.21, 29.16, 26.00, 22.68, 14.12. IR $\bar{\nu}$ cm⁻¹: 2921, 2849 (C-H, sp²), 2225 (C≡N stretch), 1622 (C=N), 1607 (para disubstituted benzene), 1512, 1255, 1164, 812, 540. Elemental Analysis for C₄₁H₄₈N₂O Calculated: C = 84.20 %, H = 8.27 %, N = 4.79 %; Found: C = 84.14 %, H = 8.24 %, N = 4.67 %.

CB80.8: ^1H NMR (400 MHz, CDCl_3) δ ppm: 8.42 (s, 1H, $\text{CH}=\text{N}$), 7.84 (d, $J = 8.7$ Hz, 2H, Ar), 7.71 (m, 4H, Ar), 7.53 (d, $J = 8.2$ Hz, 2H, Ar), 7.31 (d, $J = 8.2$ Hz, 2H, Ar), 7.21 (d, $J = 8.3$ Hz, 2H, Ar), 7.15 (d, $J = 8.3$ Hz, 2H, Ar), 6.98 (d, $J = 8.7$ Hz, 2H, Ar), 4.04 (t, $J = 6.5$ Hz, 2H, $\text{ArCH}_2\text{CH}_2\text{CH}_2\text{CH}_2\text{CH}_2\text{CH}_2\text{CH}_2\text{OAr}$), 2.75–2.60 (m, 4H, $\text{ArCH}_2(\text{CH}_2)_7\text{OAr}$, $\text{ArCH}_2(\text{CH}_2)_6\text{CH}_3$), 1.83 (p, $J = 6.6$ Hz, 2H, $\text{Ar}(\text{CH}_2)_6\text{CH}_2\text{CH}_2\text{OAr}$), 1.72–1.60 (m, 4H, $\text{ArCH}_2\text{CH}_2(\text{CH}_2)_6\text{OAr}$, $\text{ArCH}_2\text{CH}_2(\text{CH}_2)_6\text{CH}_3$), 1.55–1.24 (m, 18H, $\text{ArCH}_2\text{CH}_2\text{CH}_2\text{CH}_2\text{CH}_2\text{CH}_2\text{CH}_2\text{CH}_2\text{OAr}$, $\text{ArCH}_2\text{CH}_2\text{CH}_2\text{CH}_2\text{CH}_2\text{CH}_2\text{CH}_2\text{CH}_2\text{CH}_3$), 0.91 (t, $J = 7.4$ Hz, 3H, $\text{ArCH}_2\text{CH}_2\text{CH}_2\text{CH}_2\text{CH}_2\text{CH}_2\text{CH}_2\text{CH}_2\text{CH}_3$). ^{13}C NMR (101 MHz, CDCl_3) δ ppm: 161.70, 158.97, 149.98, 145.62, 143.72, 140.45, 136.42, 132.58, 130.37, 129.26, 129.19, 129.08, 127.49, 127.10, 120.76, 119.12, 114.66, 110.55, 68.13, 35.62, 35.19, 33.73, 32.54, 31.36, 29.39, 29.26, 29.21, 29.15, 26.00, 22.37, 13.98. IR $\bar{\nu}$ cm^{-1} : 2919, 2849 (C-H, sp^2), 2224 ($\text{C}\equiv\text{N}$ stretch), 1622 (C=N), 1606 (para disubstituted benzene), 1511, 1248, 1164, 817, 539. Elemental Analysis for $\text{C}_{42}\text{H}_{50}\text{N}_2\text{O}$ Calculated: C = 84.23 %, H = 8.42 %, N = 4.68 %; Found: C = 84.18 %, H = 8.31 %, N = 4.32 %.

CB80.9: ^1H NMR (400 MHz, CDCl_3) δ ppm: 8.42 (s, 1H, $\text{CH}=\text{N}$), 7.84 (d, $J = 8.7$ Hz, 2H, Ar), 7.71 (m, 4H, Ar), 7.53 (d, $J = 8.2$ Hz, 2H, Ar), 7.31 (d, $J = 8.2$ Hz, 2H, Ar), 7.21 (d, $J = 8.3$ Hz, 2H, Ar), 7.15 (d, $J = 8.3$ Hz, 2H, Ar), 6.98 (d, $J = 8.8$ Hz, 2H, Ar), 4.04 (t, $J = 6.5$ Hz, 2H, $\text{ArCH}_2\text{CH}_2\text{CH}_2\text{CH}_2\text{CH}_2\text{CH}_2\text{CH}_2\text{OAr}$), 2.73–2.60 (m, 4H, $\text{ArCH}_2(\text{CH}_2)_7\text{OAr}$, $\text{ArCH}_2\text{CH}_2(\text{CH}_2)_4\text{CH}_2\text{CH}_2\text{CH}_3$), 1.83 (p, $J = 6.7$ Hz, 2H, $\text{Ar}(\text{CH}_2)_6\text{CH}_2\text{CH}_2\text{OAr}$), 1.71–1.59 (m, 4H, $\text{ArCH}_2\text{CH}_2(\text{CH}_2)_6\text{OAr}$, $\text{ArCH}_2\text{CH}_2(\text{CH}_2)_4\text{CH}_2\text{CH}_2\text{CH}_3$), 1.55–1.14 (m, 20H, $\text{ArCH}_2\text{CH}_2\text{CH}_2\text{CH}_2\text{CH}_2\text{CH}_2\text{CH}_2\text{CH}_2\text{OAr}$, $\text{ArCH}_2\text{CH}_2(\text{CH}_2)_4\text{CH}_2\text{CH}_2\text{CH}_3$), 0.91 (t, $J = 6.8$ Hz, 3H, $\text{ArCH}_2\text{CH}_2(\text{CH}_2)_4\text{CH}_2\text{CH}_2\text{CH}_3$). ^{13}C NMR (101 MHz, CDCl_3) δ ppm: 161.70, 158.96, 149.93, 145.62, 143.72, 140.51, 136.50, 132.58, 130.37, 129.26, 129.19, 129.07, 127.49, 127.10, 120.67, 119.06, 114.66, 110.56, 68.13, 35.62, 35.51, 31.92, 31.59, 31.36, 29.58, 29.54, 29.39, 29.34, 29.27, 29.21, 29.16, 26.00, 22.70, 14.13. IR $\bar{\nu}$ cm^{-1} : 2918, 2847 (C-H, sp^2), 2232 ($\text{C}\equiv\text{N}$ stretch), 1623 (C=N), 1603 (para disubstituted benzene), 1510, 1254, 1162, 815, 540. Elemental Analysis for $\text{C}_{43}\text{H}_{52}\text{N}_2\text{O}$ Calculated: C = 84.27 %, H = 8.55 %, N = 4.57 %; Found: C = 84.27 %, H = 8.47 %, N = 4.40 %.

CB80.10: ^1H NMR (400 MHz, CDCl_3) δ ppm: 8.42 (s, 1H, $\text{CH}=\text{N}$), 7.85 (d, $J = 8.7$ Hz, 2H, Ar), 7.71 (m, 4H, Ar), 7.53 (d, $J = 8.2$ Hz, 2H, Ar), 7.32 (d, $J = 8.1$ Hz, 2H, Ar), 7.21 (d, $J = 8.3$ Hz, 2H, Ar), 7.15 (d, $J = 8.3$ Hz, 2H, Ar), 6.98 (d, $J = 8.7$ Hz, 2H, Ar), 4.04 (t, $J = 6.5$ Hz, 2H, $\text{ArCH}_2\text{CH}_2\text{CH}_2\text{CH}_2\text{CH}_2\text{CH}_2\text{CH}_2\text{OAr}$), 2.73–2.60 (m, 4H, $\text{ArCH}_2(\text{CH}_2)_7\text{OAr}$, $\text{ArCH}_2\text{CH}_2(\text{CH}_2)_7\text{CH}_3$), 1.82 (p, $J = 6.7$ Hz, 2H, $\text{Ar}(\text{CH}_2)_6\text{CH}_2\text{CH}_2\text{OAr}$), 1.74–1.59 (m, 4H, $\text{ArCH}_2\text{CH}_2(\text{CH}_2)_6\text{OAr}$, $\text{ArCH}_2\text{CH}_2(\text{CH}_2)_7\text{CH}_3$), 1.56–1.26 (m, 22H, $\text{ArCH}_2\text{CH}_2\text{CH}_2\text{CH}_2\text{CH}_2\text{CH}_2\text{CH}_2\text{CH}_2\text{OAr}$, $\text{ArCH}_2\text{CH}_2(\text{CH}_2)_7\text{CH}_3$), 0.91 (t, $J = 7.0$ Hz, 3H, $\text{ArCH}_2\text{CH}_2(\text{CH}_2)_7\text{CH}_3$). ^{13}C NMR (101 MHz, CDCl_3) δ ppm: 161.71, 159.02, 149.90, 145.63, 143.72, 140.53, 136.49, 132.58, 130.39, 129.23, 129.20, 129.08, 127.49, 127.10, 120.77, 119.06, 114.67, 110.54, 68.14, 35.62, 35.51, 31.92, 31.59, 31.36, 29.64, 29.63, 29.54, 29.39, 29.35, 29.33, 29.27, 29.21, 29.16, 26.00, 22.70, 14.14. IR $\bar{\nu}$ cm^{-1} : 2918, 2849 (C-H, sp^2), 2228 ($\text{C}\equiv\text{N}$ stretch), 1622 (C=N), 1607 (para disubstituted benzene), 1512, 1251, 1169, 812, 538. Elemental Analysis for $\text{C}_{44}\text{H}_{54}\text{N}_2\text{O}$ Calculated: C = 84.30 %, H = 8.68 %, N = 4.47 %; Found: C = 83.99 %, H = 8.75 %, N = 4.35 %.

CB80.11: ^1H NMR (400 MHz, CDCl_3) δ ppm: 8.42 (s, 1H, $\text{CH}=\text{N}$), 7.84 (d, $J = 8.7$ Hz, 2H, Ar), 7.73 (m, 4H, Ar), 7.53 (d, $J = 8.1$ Hz, 2H, Ar), 7.31 (d, $J = 8.2$ Hz, 2H, Ar), 7.21 (d, $J = 8.2$ Hz, 2H, Ar), 7.15 (d, $J = 8.3$ Hz, 2H, Ar), 6.98 (d, $J = 8.7$ Hz, 2H, Ar), 4.04 (t, $J = 6.5$ Hz, 2H, $\text{ArCH}_2\text{CH}_2\text{CH}_2\text{CH}_2\text{CH}_2\text{CH}_2\text{CH}_2\text{OAr}$), 2.73–2.60 (m, 4H, $\text{ArCH}_2(\text{CH}_2)_7\text{OAr}$, $\text{ArCH}_2\text{CH}_2(\text{CH}_2)_8\text{CH}_3$), 1.83 (p, $J = 6.6$ Hz, 2H, $\text{Ar}(\text{CH}_2)_6\text{CH}_2\text{CH}_2\text{OAr}$), 1.72–1.59 (m, 4H, $\text{ArCH}_2\text{CH}_2(\text{CH}_2)_6\text{OAr}$, $\text{ArCH}_2\text{CH}_2(\text{CH}_2)_8\text{CH}_3$), 1.56–1.06 (m, 24H, $\text{ArCH}_2\text{CH}_2\text{CH}_2\text{CH}_2\text{CH}_2\text{CH}_2\text{CH}_2\text{CH}_2\text{OAr}$, $\text{ArCH}_2\text{CH}_2(\text{CH}_2)_8\text{CH}_3$), 0.91 (t, $J = 6.7$ Hz, 3H, $\text{ArCH}_2\text{CH}_2(\text{CH}_2)_8\text{CH}_3$). ^{13}C NMR (101 MHz, CDCl_3) δ ppm: 161.70, 158.96, 149.93, 145.62, 143.72, 140.51, 136.50, 132.58, 130.37, 129.26, 129.20, 129.07, 127.49, 127.10, 120.76, 119.06, 114.66, 110.56, 68.13, 35.62, 35.51, 31.94, 31.59, 31.36, 29.69, 29.65, 29.62, 29.54, 29.39, 29.36, 29.33, 29.27, 29.21, 29.16, 26.00, 22.71,

14.14. IR $\bar{\nu}$ cm⁻¹: 2918, 2848 (C-H, sp²), 2227 (C≡N stretch), 1622 (C=N), 1607 (para disubstituted benzene), 1512, 1250, 1169, 814, 541.

CB80.12: ¹H NMR (400 MHz, CDCl₃) δ ppm: 8.42 (s, 1H, CH=N), 7.84 (d, J = 8.7 Hz, 2H, Ar), 7.71 (m, 4H, Ar), 7.53 (d, J = 8.2 Hz, 2H, Ar), 7.31 (d, J = 8.1 Hz, 2H, Ar), 7.21 (d, J = 8.2 Hz, 2H, Ar), 7.15 (d, J = 8.3 Hz, 2H, Ar), 6.98 (d, J = 8.7 Hz, 2H, Ar), 4.04 (t, J = 6.5 Hz, 2H, ArCH₂CH₂CH₂CH₂CH₂CH₂CH₂CH₂OAr), 2.73–2.59 (m, 4H, ArCH₂(CH₂)₇OAr, ArCH₂CH₂(CH₂)₉CH₃), 1.83 (p, J = 6.6 Hz, 2H, Ar(CH₂)₆CH₂CH₂OAr), 1.72–1.59 (m, 4H, ArCH₂CH₂(CH₂)₆OAr, ArCH₂CH₂(CH₂)₉CH₃), 1.57–1.14 (m, 26H, ArCH₂CH₂CH₂CH₂CH₂CH₂CH₂CH₂CH₂OAr, ArCH₂CH₂(CH₂)₉CH₃), 0.90 (t, J = 6.7 Hz, 3H, ArCH₂CH₂(CH₂)₉CH₃). ¹³C NMR (101 MHz, CDCl₃) δ ppm: 161.72, 159.04, 149.88, 145.62, 143.72, 140.54, 136.49, 132.58, 130.40, 129.22, 129.20, 129.09, 127.49, 127.10, 120.78, 119.06, 114.67, 110.53, 68.14, 35.63, 35.52, 31.95, 31.59, 31.36, 29.71, 29.69, 29.67, 29.63, 29.55, 29.40, 29.38, 29.34, 29.27, 29.22, 29.16, 26.00, 22.72, 14.15. IR $\bar{\nu}$ cm⁻¹: 2917, 2850 (C-H, sp²), 2228 (C≡N stretch), 1625 (C=N), 1605 (para disubstituted benzene), 1512, 1258, 1162, 817, 538. HRMS: (TOF ESI+) (m/z): [M+H]⁺ for C₄₆H₅₉N₂O Calculated: 655.4627; Found: 655.4608 (2.9 ppm difference).

CB80.14: ¹H NMR (400 MHz, CDCl₃) δ ppm: 8.42 (s, 1H, CH=N), 7.84 (d, J = 8.7 Hz, 2H, Ar), 7.71 (m, 4H, Ar), 7.53 (d, J = 8.2 Hz, 2H, Ar), 7.31 (d, J = 8.1 Hz, 2H, Ar), 7.21 (d, J = 8.3 Hz, 2H, Ar), 7.15 (d, J = 8.3 Hz, 2H, Ar), 6.85 (d, J = 8.5 Hz, 2H, Ar), 4.04 (t, J = 6.5 Hz, 2H, ArCH₂CH₂CH₂CH₂CH₂CH₂CH₂CH₂OAr), 2.73–2.59 (m, 4H, ArCH₂(CH₂)₇OAr, ArCH₂CH₂(CH₂)₁₁CH₃), 1.83 (p, J = 6.7 Hz, 2H, Ar(CH₂)₆CH₂CH₂OAr), 1.76–1.62 (m, 4H, ArCH₂CH₂(CH₂)₆OAr, ArCH₂CH₂(CH₂)₁₁CH₃), 1.55–1.06 (m, 30H, ArCH₂CH₂CH₂CH₂CH₂CH₂CH₂CH₂CH₂OAr, ArCH₂CH₂(CH₂)₁₁CH₃), 0.90 (t, J = 6.7 Hz, 3H, Ar(CH₂)₁₃CH₃). ¹³C NMR (101 MHz, CDCl₃) δ ppm: 161.70, 158.97, 149.92, 145.62, 143.72, 140.52, 136.49, 132.58, 130.38, 129.26, 129.20, 129.08, 127.49, 127.10, 120.77, 119.06, 114.66, 110.55, 68.13, 35.63, 35.52, 31.95, 31.59, 31.37, 29.72, 29.71, 29.63, 29.55, 29.39, 29.34, 29.27, 29.22, 29.17, 26.00, 22.72, 14.15. IR $\bar{\nu}$ cm⁻¹: 2915, 2847 (C-H, sp²), 2237 (C≡N stretch), 1621 (C=N), 1607 (para disubstituted benzene), 1510, 1250, 1166, 816, 541. HRMS: (TOF ESI+) (m/z): [M+H]⁺ for C₄₈H₆₃N₂O Calculated: 683.4940; Found: 683.4924 (2.3 ppm difference).

CB80.16: ¹H NMR (400 MHz, CDCl₃) δ ppm: 8.42 (s, 1H, CH=N), 7.84 (d, J = 8.7 Hz, 2H, Ar), 7.71 (m, 4H, Ar), 7.53 (d, J = 8.1 Hz, 2H, Ar), 7.31 (d, J = 8.1 Hz, 2H, Ar), 7.21 (d, J = 8.3 Hz, 2H, Ar), 7.15 (d, J = 8.3 Hz, 2H, Ar), 6.98 (d, J = 8.7 Hz, 2H, Ar), 4.04 (t, J = 6.5 Hz, 2H, ArCH₂CH₂CH₂CH₂CH₂CH₂CH₂CH₂OAr), 2.73–2.59 (m, 4H, ArCH₂(CH₂)₇OAr, ArCH₂CH₂(CH₂)₁₃CH₃), 1.83 (p, J = 6.7 Hz, 2H, Ar(CH₂)₆CH₂CH₂OAr), 1.65 (m, 4H, ArCH₂CH₂(CH₂)₆OAr, ArCH₂CH₂(CH₂)₁₃CH₃), 1.34 (m, 34H, ArCH₂CH₂CH₂CH₂CH₂CH₂CH₂CH₂CH₂OAr, ArCH₂CH₂(CH₂)₁₃CH₃), 0.90 (t, J = 6.7 Hz, 3H, ArCH₂CH₂(CH₂)₁₃CH₃). ¹³C NMR (101 MHz, CDCl₃) δ ppm: 161.70, 158.97, 149.92, 145.62, 143.72, 140.52, 136.50, 132.58, 130.37, 129.25, 129.19, 129.07, 127.49, 127.10, 120.76, 119.06, 114.66, 110.55, 68.13, 35.62, 35.51, 31.94, 31.59, 31.36, 29.72, 29.62, 29.54, 29.38, 29.33, 29.27, 29.21, 29.16, 22.71, 14.14. IR $\bar{\nu}$ cm⁻¹: 2915, 2847 (C-H, sp²), 2237 (C≡N stretch), 1621 (C=N), 1607 (para disubstituted benzene), 1510, 1250, 1166, 816, 541. HRMS: (TOF ESI+) (m/z): [M+H]⁺ for C₅₀H₆₇N₂O Calculated: 711.5253; Found: 711.5261 (1.1 ppm difference).

CB80.18: ¹H NMR (400 MHz, CDCl₃) δ ppm: 8.42 (s, 1H, CH=N), 7.84 (d, J = 8.7 Hz, 2H, Ar), 7.71 (m, 4H, Ar), 7.53 (d, J = 8.1 Hz, 2H, Ar), 7.31 (d, J = 8.1 Hz, 2H, Ar), 7.21 (d, J = 8.2 Hz, 2H, Ar), 7.15 (d, J = 8.3 Hz, 2H, Ar), 6.98 (d, J = 8.7 Hz, 2H, Ar), 4.04 (t, J = 6.5 Hz, 2H, ArCH₂CH₂CH₂CH₂CH₂CH₂CH₂CH₂OAr), 2.73–2.59 (m, 4H, ArCH₂(CH₂)₇OAr, ArCH₂CH₂(CH₂)₁₅CH₃), 1.83 (p, J = 6.7 Hz, 2H, Ar(CH₂)₆CH₂CH₂OAr), 1.70–1.59 (m, 4H, ArCH₂CH₂(CH₂)₆OAr, ArCH₂CH₂(CH₂)₁₅CH₃), 1.54–1.18 (m, 38H, ArCH₂CH₂CH₂CH₂CH₂CH₂CH₂CH₂CH₂OAr, ArCH₂CH₂(CH₂)₁₅CH₃), 0.90 (t, J = 6.8 Hz, 3H, ArCH₂CH₂(CH₂)₁₅CH₃). ¹³C NMR (101 MHz, CDCl₃) δ ppm: 161.70, 158.97, 149.92, 145.62, 143.72, 140.51, 136.50, 132.58, 130.37, 129.26, 129.19, 129.07, 127.49, 127.10, 120.76, 119.06, 114.66,

110.55, 68.13, 35.62, 35.51, 31.94, 31.59, 31.36, 29.72, 29.63, 29.54, 29.38, 29.34, 29.27, 29.21, 29.16, 26.00, 22.71, 14.14. IR $\bar{\nu}$ cm⁻¹: 2917, 2850 (C-H, sp²), 2239 (C≡N stretch), 1621 (C=N), 1607 (para disubstituted benzene), 1513, 1259, 1163, 817, 540. HRMS: (TOF ESI+) (m/z): [M+H]⁺ for C₅₂H₇₁N₂O Calculated: 739.5566; Found: 739.5581 (2.0 ppm difference).

2. Additional Optical birefringence

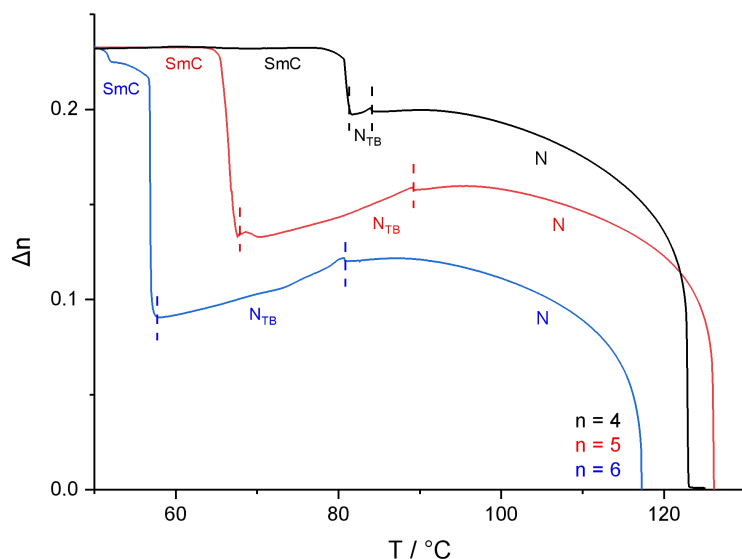


Figure S1. Optical birefringence as a function of temperature for CB80.4, CB80.5 and CB80.6.

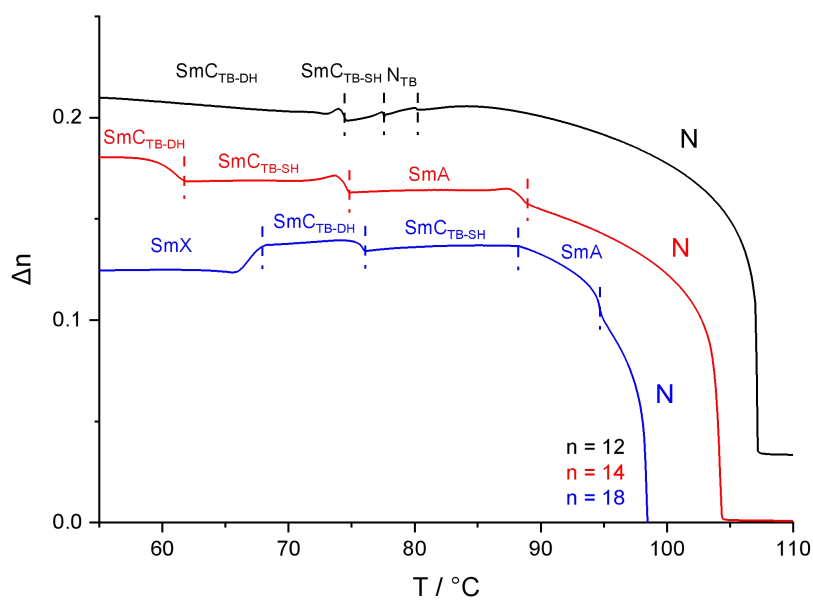


Figure S2. Optical birefringence as a function of temperature for CB80.12, CB80.14 and CB80.18.

3. Additional X-ray diffraction

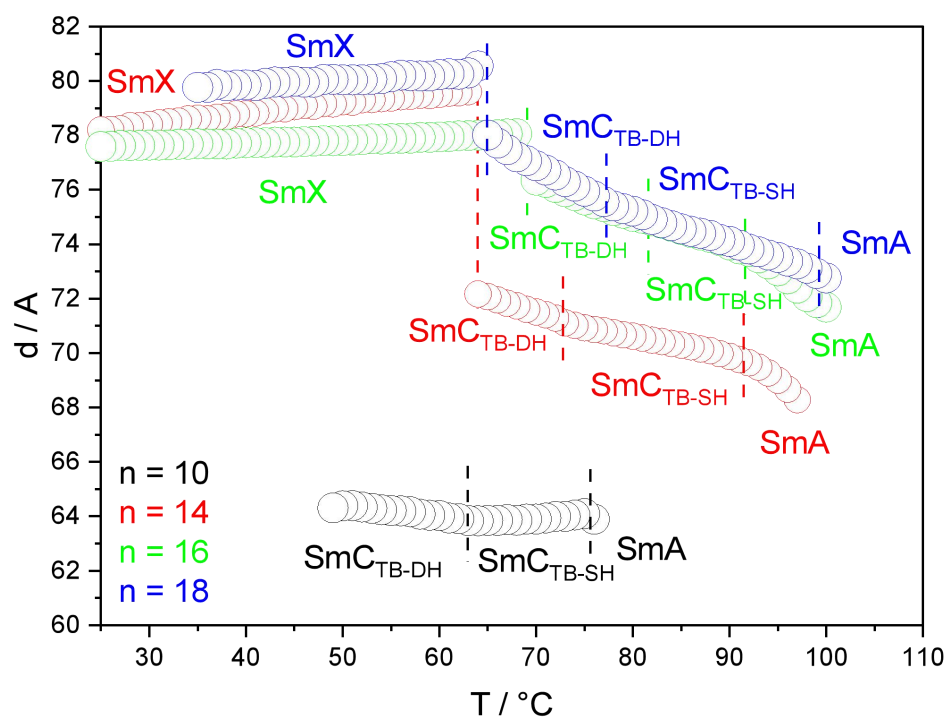


Figure S3. The temperature dependence of the layer spacings shown for the smectic phases exhibited by $CB40.m$ homologues with $m = 10, 14, 16, 18$.

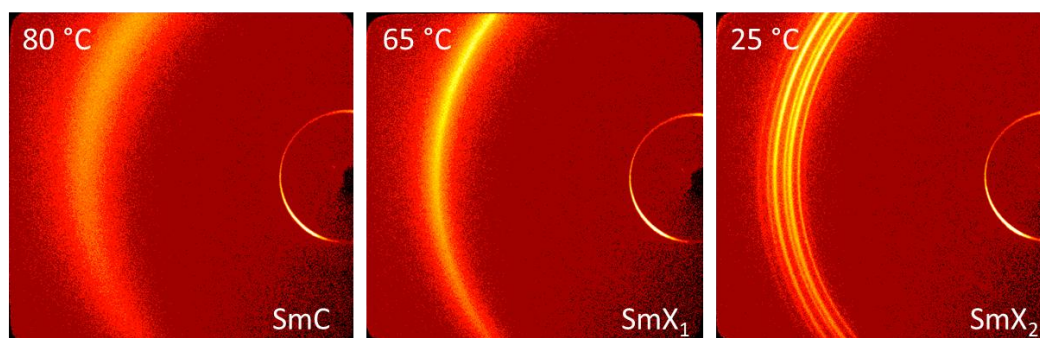


Figure S4. X-ray diffraction patterns for $CB80.4$ in SmC and higher order phases arbitrarily named SmX_1 and SmX_2 .

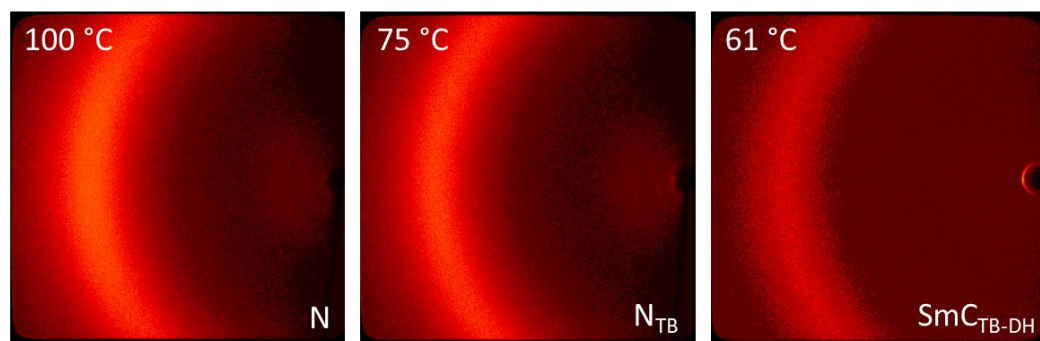


Figure S5. X-ray diffraction patterns for $CB80.11$ in N , N_{TB} and SmC_{TB-DH} phases.